JOURNAL OF GUIDANCE, CONTROL, AND DYNAMICS
Vol. 33, No. 4, July–August 2010

Lyapunov-Based Thrusters' Selection for Spacecraft Control: Analysis and Experimentation

Fabio Curti
University of Rome "La Sapienza," 00184 Rome, Italy
and
Marcello Romano and Riccardo Bevilacqua
Naval Postgraduate School, Monterey, California 93943

DOI: 10.2514/1.47296

This paper introduces a method for spacecraft rotation and translation control by on–off thrusters with guaranteed Lyapunov-stable tracking of linear dynamic models. In particular, the proposed control method switches on, at each time step, only those thrusters needed to maintain stability. Furthermore, the strategy allocates the configuration so that the minimum number of actuators is used. One of the benefits of the proposed method is that it substitutes both the thruster mapping and the pulse modulation algorithms typically used for real-time allocation of the firing thrusters and for determining the duration of the firing. The proposed approach reduces the computational burden of the onboard computer versus the use of classical thruster mapping algorithms, which typically involve iterative matrix operations. The paper presents analytical demonstrations, numerical simulations on a six-degree-of-freedom spacecraft, and experimental tests on a hardware-in-the-loop three-degree-of-freedom spacecraft simulator floating over air pads on a flat floor. The method proves to be effective and easy to implement in real time.

Fabio Curti is an Associate Professor at the School of Aerospace Engineering of the University of Rome "La Sapienza." His main research interests are space robotics, spacecraft attitude, determination and control, and space navigation, rendezvous, and docking. He received his M.S. degree in control engineering from the University of Rome "La Sapienza," in 1989. From 1989 to 1991, he participated in the international study of shape and attitude control of large space structures at the San Marco Project. From 1991 to 1992, he was employed with the Telespazio Company in the Space System Division, Space Technology Department, as a Space System Engineer. From 1992 to 2005, he was an Assistant Professor at the School of Aerospace Engineering. As a Visiting Professor, from 2003 to 2006, he was at the School of Engineering of the University of Bologna. Between 1997 and 2005, Fabio Curti was involved in the Malindi Ground Station (San Marco Project, "La Sapienza"—Kenya) in mission supports for launchers and low early-orbit phase operations for national and international satellites. He is the founder of the Automation, Control, and Robotics for Aerospace Laboratory at the Aerospace and Astronautical Engineering Department. Fabio Curti is a Member of the AIAA.

Marcello Romano is an Associate Fellow of the AIAA. He received his M.S. and Ph.D. in Aerospace Engineering from Politecnico di Milano, in 1997 and 2001, respectively. Since 2004, he has been an Assistant Professor at the Naval Postgraduate School, in the Department of Mechanical and Aerospace Engineering and in the Space Systems Academic Group. His research interests are in spacecraft dynamics, guidance, and control; robotics; and nanosatellite systems.

Riccardo Bevilacqua is an Associate Fellow of the U.S. National Research Council in Mechanical and Aerospace Engineering Department of the Naval Postgraduate School. He manages the Spacecraft Robotics Laboratory. Dr. Bevilacqua's main research interests are in the dynamics and control of multiple autonomous spacecraft and robotic systems. He received his M.S. in aerospace engineering in 2002 and his Ph.D. in applied mathematics in 2007, both from the University of Rome "La Sapienza". He was a Project Engineer at the Grupo Mecanica del Vuelo, during 2003 and a Principal Investigator of the ESA's Ariadna Research Project in 2003. Dr. Bevilacqua is a Member of AIAA.

Received 21 September 2009; revision received 10 March 2010; accepted for publication 12 March 2010.

Nomenclature

A_m	=	reference model dynamics matrix
$B(\underline{\sigma})$	=	control distribution matrix
$\underline{e}$	=	tracking error vector
H	=	thrust distribution matrix
$\underline{F}_c$	=	control forces
$\underline{M}_c$	=	control torques
P	=	solution matrix of the Lyapunov equation
Q	=	selected Lyapunov equation matrix
R	=	rotation matrix
$S(a)$	=	switching function
$\underline{u}$	=	thrusts' vector
V	=	Lyapunov function
$\underline{v}_{\rho c}$	=	inputs' vector of the commanded trajectory
$\underline{v}_{\sigma c}$	=	inputs' vector of the commanded attitude maneuver
$\underline{w}$	=	ideal control vector
$\underline{\beta}_\rho$, $\underline{\beta}_\sigma$	=	thrusters' activation vectors
$\underline{\gamma}_\rho$, $\underline{\gamma}_\sigma$	=	functions of tracking errors
Δ_ρ, Δ_σ	=	terms of the derivative of the Lyapunov functions
$\underline{\varepsilon}_\rho$	=	position tracking error vector
$\underline{\varepsilon}_\sigma$	=	modified Rodrigues parameters tracking error vector
$\underline{\varphi}$, $\underline{\pi}$	=	switching variables' vectors
$\underline{\rho}$	=	relative position vector
$\underline{\sigma}$	=	modified Rodrigues parameters vector
$\underline{\omega}$	=	angular velocity vector of the space vehicle with respect to Earth-centered inertial reference frame in spacecraft reference frame coordinates
ϖ	=	command frequency
$\underline{\omega}_L$	=	angular velocity vector of the local-vertical–local-horizontal frame with respect to Earth-centered inertial reference frame in local-vertical–local-horizontal coordinates

I. Introduction

CONTROL of space vehicles for proximity operations, such as rendezvous and docking, is a problem of great interest for future manned missions [1], autonomous guidance of satellite swarms [2], onorbit servicing missions operated by free-flyer robotic spacecraft for refueling, monitoring or removing satellites [3–5], or for the autonomous onorbit assembly of a large space structure [6].

For some of these applications, it may be necessary to control the rotational and translational motions by the use of on–off thrusters. The use of thrusters as the only actuators to steer the space vehicle leads to dynamic coupling between rotation and translation.

Commonly, the control scheme for a spacecraft is based on continuous control laws, designed with either linear or nonlinear methods, which provide the necessary forces and torques to pursue programmed trajectories and attitude maneuvers of the space vehicle. As a result, the designed continuous control forces and torques have to be mapped into thrusters' forces. This is accomplished by applying thruster mapping strategies that are usually based on the simplex method [7]. Because of the thrusters' on–off nature, the output of the thruster mapping algorithm is the input of the pulse-width modulator that modulates a continuous thrust in a pulsed thrust aimed at minimizing the difference between the actual pulsed control and the designed continuous control [8–10].

The problem of control in the presence of actuator saturation limits has been dealt with in the past [11] and the global stability has been verified for a class of model reference adaptive controllers [12]. Moreover, an adaptive control law has been developed to asymptotically enforce desired closed-loop dynamics by using the Lyapunov approach [13]. In the present work the Lyapunov approach is applied to search the suitable thrusters' commanding strategy so that the rotational and relative translational dynamics are tracking linear reference models. As result, the control problem with on–off actuators is simplified, since position and attitude maneuvers can be designed upon the reference models by using the linear control theory.

Furthermore, the number of thrusters to be activated is minimized. The thrusters' configuration is at each time step chosen, which maintains the derivative of the Lyapunov function negative while the space vehicle dynamics tracks a linear reference model. The proposed approach reduces the complexity of the control scheme because the simplex method and the pulse-width modulator are replaced with a Lyapunov-based thrusters' selection strategy. Such strategy uses functions of the difference between the linear reference model state vector and the actual dynamics state vector, and it produces the thrusters' on–off commands.

The paper is organized as follows. In Sec. II, the spacecraft rototranslational dynamics equations are formulated in a mobile orbital frame when only thrusters are the actuators for the control. In Sec. III, the Lyapunov approach is presented. In Sec. IV, the proposed method is numerically tested in simulation for the control of the rotational and translational dynamics of a space vehicle. In Sec. V, the proposed method is experimentally tested on one of the spacecraft simulators of the Spacecraft Robotics Laboratory at the Naval Postgraduate School [14]. Section VI concludes the paper.

II. Space Vehicle Dynamics with Thrusters-Only Actuation

This section deals with the rototranslational dynamics equations for a space vehicle. In particular, we use the local-vertical–local-horizontal (LVLH) reference frame, since the main application of the proposed method is considered to be in proximity maneuvers of spacecraft.

A. Reference Frames

The following coordinate frames are used (Fig. 1):

1. The first coordinate frame is the LVLH reference frame (LRF) attached to an orbiting reference point, with x axis directed along the radius vector $\underline{r}_L$ of the reference point from the Earth's center z axis in the direction of the orbit normal and y axis directed to complete the right-handed coordinate frame;

2. The second coordinate frame is the spacecraft reference frame (SRF), which is the body principal axes of inertia frame of the spacecraft.

The rotation matrices between the two coordinate frames are denoted with ${}^S R_L$.

B. Rototranslational Dynamics

The rotational dynamics are governed by the classical Euler equations of the rigid body and the attitude kinematics has different expressions according to the attitude parameterization.

Relative translational dynamics are developed as the relative position and translational velocity of the spacecraft with respect to the origin of the LVLH reference frame.

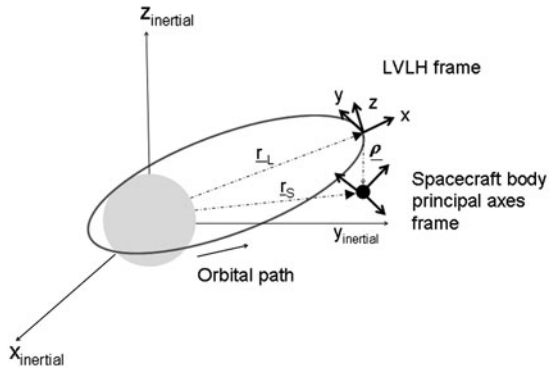

Fig. 1 Reference frames: inertial, LVLH, and spacecraft body principal axes.

1. Rotational Dynamics

We use the modified Rodrigues parameters (MRPs) for the attitude representation because they minimize the attitude parameters [15] and, as we show below, can be useful to write the attitude dynamics in a general manner as nonlinear second-order differential equations.

The rotational kinematics of SRF with respect to LRF is expressed in terms of MRPs $\underline{\sigma}^T = [\,\sigma_1 \quad \sigma_2 \quad \sigma_3\,]$ by the following equation [16]:

$$\dot{\underline{\sigma}} = \tfrac{1}{4} C(\underline{\sigma})[\underline{\omega} - {}^S R_L(\underline{\sigma})\underline{\omega}_L] \tag{1}$$

where $\underline{\omega}$ is the absolute angular velocity vector of the vehicle expressed in SRF, $\underline{\omega}_L$ is the absolute angular velocity vector of the LRF, while

$${}^S R_L(\underline{\sigma}) = I_{3\times 3} + \frac{8[\tilde{\underline{\sigma}}]^2 - 4(1 - \underline{\sigma}^T\underline{\sigma})[\tilde{\underline{\sigma}}]}{(1 + \underline{\sigma}^T\underline{\sigma})^2} \tag{2}$$

is the rotation matrix from the LRF to SRF, and

$$C(\underline{\sigma}) = [(1 - \underline{\sigma}^T\underline{\sigma})I_{3\times 3} + 2[\tilde{\underline{\sigma}}] + 2\underline{\sigma}\underline{\sigma}^T] \tag{3}$$

In Eq. (3), and in the following, the tilde symbol $[\tilde{\underline{s}}]$ applied to a generic vector $\underline{s} = [\,s_1 \quad s_2 \quad s_3\,]^T$ is the skew symmetric matrix form, representing the cross product in matrix algebra:

$$[\tilde{\underline{s}}] = \begin{pmatrix} 0 & -s_3 & s_2 \\ s_3 & 0 & -s_1 \\ -s_2 & s_1 & 0 \end{pmatrix} \tag{4}$$

The rotational dynamics for a rigid body is

$$\dot{\underline{\omega}} = J^{-1}([\tilde{\underline{\omega}}]J\underline{\omega} + {}^S\underline{M}_c) \tag{5}$$

where $J = \mathrm{diag}(\,J_1 \quad J_2 \quad J_3\,)$ is the diagonal matrix of the principal moments of inertia and ${}^S\underline{M}_c$ is the vector of the control torques around the principal axes of inertia in the SRF. From Eq. (1) the angular velocity can be expressed as a function of $\underline{\sigma}$, $\dot{\underline{\sigma}}$ and $\underline{\omega}_L$ as

$$\underline{\omega} = \frac{4}{(1 + \underline{\sigma}^T\underline{\sigma})^2} C^T(\underline{\sigma})\dot{\underline{\sigma}} + {}^S R_L(\underline{\sigma})\underline{\omega}_L \tag{6}$$

because

$$C^{-1}(\underline{\sigma}) = \frac{C^T(\underline{\sigma})}{(1 + \underline{\sigma}^T\underline{\sigma})^2} \tag{7}$$

By taking the derivative of Eq. (1) and using Eqs. (5) and (6), it yields:

$$\ddot{\underline{\sigma}} = \underline{f}(\underline{\sigma}, \dot{\underline{\sigma}}, \underline{\omega}_L, \dot{\underline{\omega}}_L) + G(\underline{\sigma}){}^S\underline{M}_c \tag{8}$$

which is a system of nonlinear second-order differential equations, where the matrix $G(\underline{\sigma}) = \frac{1}{4}\cdot C(\underline{\sigma})J^{-1}$ is invertible and $\underline{f}(\underline{\sigma}, \dot{\underline{\sigma}}, \underline{\omega}_L, \dot{\underline{\omega}}_L)$ is a vector nonlinear function. Equation (8) is the attitude dynamics equation expressed as a function of MRPs, their time derivatives, and the kinematics of LRF.

2. Translational Dynamics

The relative position of the center of mass of the spacecraft can be expressed in terms of Cartesian coordinates $\underline{\rho} = [\,x \quad y \quad z\,]^T$ in the LRF; let $\underline{r}_S$ and $\underline{r}_L$ be the orbital position vectors of the spacecraft and the reference orbiting point, respectively, in the LRF. Then,

$$\underline{r}_S = \underline{r}_L + \underline{\rho} = \begin{bmatrix} r_L \\ 0 \\ 0 \end{bmatrix} + \begin{bmatrix} x \\ y \\ z \end{bmatrix} = \begin{bmatrix} r_L + x \\ y \\ z \end{bmatrix} \tag{9}$$

The relative translational dynamics equations are obtained based on two derivatives with respect to the inertial frame [16,17] and by considering the Keplerian motion, yielding:

$$\begin{cases} \ddot{x} = \left(\dot{\alpha}^2 - \frac{1}{\lambda}\frac{\mu_E}{r_L^3}\right)x + \ddot{\alpha}y + 2\dot{\alpha}\dot{y} + \left(1 - \frac{1}{\lambda}\right)\frac{\mu_E}{r_L^2} + \frac{1}{m}{}^L F_{cx} \\ \ddot{y} = \left(\dot{\alpha}^2 - \frac{1}{\lambda}\frac{\mu_E}{r_L^3}\right)y - \ddot{\alpha}x - 2\dot{\alpha}\dot{x} + \frac{1}{m}{}^L F_{cy} \\ \ddot{z} = -\frac{1}{\lambda}\frac{\mu_E}{r_L^3}z + \frac{1}{m}{}^L F_{cz} \end{cases} \tag{10}$$

where

$$\lambda = \left[1 + 2\frac{x}{r_L} + \left(\frac{x}{r_L}\right)^2 + \left(\frac{y}{r_L}\right)^2 + \left(\frac{z}{r_L}\right)^2\right]^{\frac{3}{2}} \tag{11}$$

The Earth gravitational constant is μ_E, and $\alpha = \theta + \upsilon$ is the true latitude of the reference orbiting point (that is, the sum of the true anomaly θ and the perigee argumentυ). ${}^L F_{cx}$, ${}^L F_{cy}$, and ${}^L F_{cz}$ are the components of the control forces vector ${}^L\underline{F}_c$ in the LVLH frame, and m is the space vehicle's mass. For a complete set of equations governing the spacecraft reference point dynamics, the equations $\ddot{\alpha} = -2(\dot{r}_L/r_L)$ and $\ddot{r}_L = r_L\dot{\alpha}^2 - (\mu_E/r_L^2)$ must be added to Eq. (10).

For the reference point in a circular orbit and $\|\rho\| \ll r_L$, Eq. (10) becomes the well-known Hill–Clohessy–Wiltshire equations [18]. The relative motion equations can be written in the following compact form:

$$\ddot{\underline{\rho}} = \underline{h}(\underline{\rho}, \dot{\underline{\rho}}) + \frac{1}{m}{}^L\underline{F}_c \tag{12}$$

where $\underline{h}(\underline{\rho}, \dot{\underline{\rho}})$ is the set of nonlinear expressions of the relative translational dynamics.

3. Rototranslational Dynamics

By looking at Eqs. (8) and (12), the rotational and translational dynamics are decoupled if the controls ${}^S\underline{M}_c$ and ${}^L\underline{F}_c$ are independent. However, in the thrusters-only case, the attitude control and the translational control are coupled and cannot be designed separately. In fact, by using the rotation matrix from the LVLH reference frame to the SRF of Eq. (2), we have ${}^L\underline{F}_c = {}^L R_S(\underline{\sigma}){}^S\underline{F}_c$, where ${}^L R_S(\underline{\sigma}) = {}^S R_L^T(\underline{\sigma}) = {}^S R_L(-\underline{\sigma})$. The required directional force ${}^S\underline{F}_c$ and torque ${}^S\underline{M}_c$ must be produced by the combined firing of the thrusters, thus these control variables are not independent.

Let $\underline{u} = u_a[\,\hat{u}_1 \quad \hat{u}_2 \quad \cdots \quad \hat{u}_n\,]^T$ be the vector of the thrusts of the thrusters, where

$$\hat{u}_i = \begin{cases} 0 & (i\text{th thruster off} \\ 1 & (i\text{th thruster on} \end{cases} \qquad i = 1, 2, \ldots, n \tag{13}$$

with u_a being the positive value of the available thrust of the thruster. The vector $\hat{\underline{u}} = [\,\hat{u}_1 \quad \hat{u}_2 \quad \cdots \quad \hat{u}_n\,]^T$ is the binary vector that we call the active thrusters' configuration at the time t.

Let us write the controls as

$$\begin{bmatrix} {}^S\underline{F}_c \\ {}^S\underline{M}_c \end{bmatrix} = \begin{bmatrix} H_F \\ H_M \end{bmatrix}\underline{u} = H\underline{u} \tag{14}$$

where H is the $6 \times n$ thrust distribution matrix related to the geometrical structure of the thrusters' placement on the spacecraft.

Let $\underline{\xi} = [\,\underline{\rho} \quad \underline{\sigma}\,]^T$ be the vector of the generalized displacements of the spacecraft, then the thruster commanded rototranslational dynamics, combining Eqs. (8), (12), and (14), has the following expression:

$$\ddot{\underline{\xi}} = \underline{p}(\underline{\xi}, \dot{\underline{\xi}}, \underline{\omega}_L, \dot{\underline{\omega}}_L) + N(\underline{\sigma})H\underline{u} \tag{15}$$

where

$$\underline{p}(\underline{\xi},\dot{\underline{\xi}},\underline{\omega}_L,\dot{\underline{\omega}}_L)=\begin{bmatrix}\underline{h}(\underline{\rho},\dot{\underline{\rho}})\\ \underline{f}(\underline{\sigma},\dot{\underline{\sigma}},\underline{\omega}_L,\dot{\underline{\omega}}_L)\end{bmatrix};\qquad N(\underline{\sigma})=\begin{bmatrix}\frac{1}{m}{}^L R_S(\underline{\sigma}) & 0_{3\times3}\\ 0_{3\times3} & G(\underline{\sigma})\end{bmatrix} \tag{16}$$

4. *Thrust Distribution Matrix Structure*

Many thrusters' architectures are possible; for instance, in [1] the problem of thrusters' placement is widely discussed for the NASA's Crew Exploration Vehicle. In general, the distribution of thrusters depends largely on the vehicle geometry and the allocation criterion [19]. In this paper, a generic fully actuated thrusters' distribution is considered, i.e., the thrusters' placement is capable of always providing directional forces and attitude control torques.

This implies that the H matrix must allow for forces and torques generation capability around the three axes of SRF [i.e., from Eq. (14)], a full rank requirement for H, otherwise a thruster configuration $\underline{u}_0 \neq \underline{0}$ exists so that $H\underline{u}_0 = 0$. Moreover, the H matrix satisfies the following properties:

1) Property 1 guarantees existence of a configuration $\underline{u}_F$ that exists, such that $H_F\underline{u}_F \neq 0$ and $H_M\underline{u}_F = 0$.

2) Property 2 guarantees existence of a configuration $\underline{u}_M$ that exists, such that $H_M\underline{u}_M \neq 0$ and $H_F\underline{u}_M = 0$.

The above-mentioned properties guarantee the capability to generate pure forces without torques and vice versa. These are intrinsic properties of the geometrical placement of the thrusters. Note that this is true only from a theoretical point of view, since systematic errors in the thrusters' placement and orientation, and slight differences of the nominal thrust among the different thrusters introduce undesired disturbance forces and torques for a given maneuver.

A sample generic structure for a fully actuated spacecraft thrusters' placement is shown in Fig. 2.

We denote with d_x, d_y, and d_z the moment arms of the thrusters with respect to the center of the mass. The thrusters are numbered from 1 through 12. For this structure, the submatrices of H, H_F, and H_M, are as follows:

$$H_F=\begin{bmatrix}-1&0&0&-1&0&0&1&0&0&1&0&0\\ 0&1&0&0&-1&0&0&1&0&0&-1&0\\ 0&0&1&0&0&-1&0&0&-1&0&0&1\end{bmatrix} \tag{17}$$

$$H_M=\begin{bmatrix}0&d_z&-d_y&0&d_z&-d_y&0&-d_z&d_y&0&-d_z&d_y\\ d_z&0&-d_x&-d_z&0&d_x&d_z&0&-d_x&-d_z&0&d_x\\ -d_y&d_x&0&d_y&-d_x&0&d_y&-d_x&0&-d_y&d_x&0\end{bmatrix} \tag{18}$$

It can be easily seen that the H matrix has full rank and satisfies properties 1 and 2. Notably, the thrusters' placement scheme of Fig. 2 is not based on the geometry of a particular space vehicle.

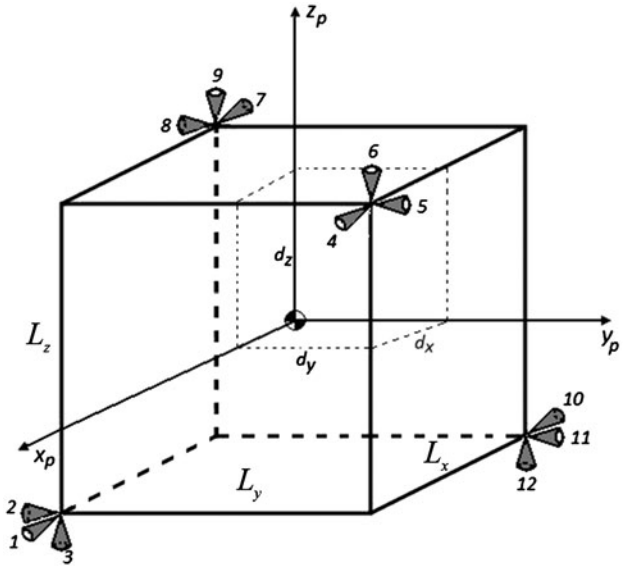

Fig. 2 Fully actuated space vehicle with thrusters only.

C. Classical Control Design Approach

The classical control design for spacecraft with only thrusters is typically conducted by solving the control problem for the rototranslational dynamics, considering the space vehicle actuated by continuous actuators. This approach leads to finding the continuous control law for ${}^S\underline{M}_c$ and ${}^S\underline{F}_c$. Subsequently, the suitable configuration of thrusters is found such that Eq. (14) is met with a minimum number of thrusters.

This problem is usually solved by applying simplex-based algorithms [20] as follows: given the known terms ${}^S\underline{M}_c$ and ${}^L\underline{F}_c$, and the attitude $\underline{\sigma}$ at the time t, let us find $\bar{\underline{u}} = [\,\bar{u}_1 \quad \bar{u}_2 \quad \cdots \quad \bar{u}_n\,]^T$, such that

$$\bar{\underline{u}}^* = \min_{\bar{u}} \sum_{i=1}^{n} \bar{u}_i$$

subject to

$$\begin{cases} u_a H_F \bar{\underline{u}} = \underline{F}_c S \\ u_a H_M \bar{\underline{u}} = \underline{M}_c S \\ 0 \le \bar{u}_i \le 1 \text{ for } i = 1, 2, \ldots, n \end{cases}$$

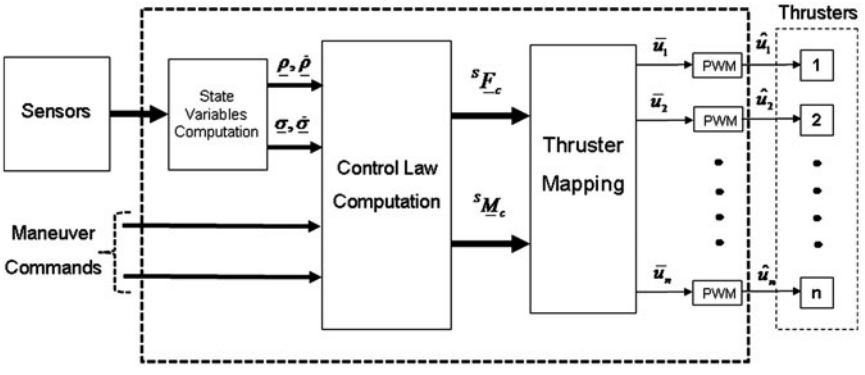

Fig. 3 Classical control block scheme for an on–off actuated spacecraft.

with ${}^{s}\underline{F}_c = {}^{S}R_L(\underline{\sigma})^{L}\underline{F}_c$. The optimal solution $\bar{\underline{u}}^*$ of the constrained minimum problem is the mapping of the force and torque control laws into positive continuous variables $\bar{u}_i^*$. The last step is to convert the continuous laws $\bar{u}_i^*$ into on–off commands $\hat{u}_i$ [Eq. (13)] by using the pulse-width-modulation (PWM) technique. The classical control schemes consist of a cascade of blocks, as shown in Fig. 3.

III. Control Design and Command Strategies Based on Reference Models

This section introduces a new thrusters' command strategy based on the tracking of the dynamics of reference linear models. The strategy is found for the generic structure of the thrusters' placement of Fig. 2.

A. Reference Model Tracking Error Equation

Let $\underline{\rho}_m$ and $\underline{\sigma}_m$ be the solutions of the following equations:

$$\ddot{\underline{\rho}}_m + K_1\dot{\underline{\rho}}_m + K_2\underline{\rho}_m = \underline{v}_{\rho c} \qquad \ddot{\underline{\sigma}}_m + K_3\dot{\underline{\sigma}}_m + K_4\underline{\sigma}_m = \underline{v}_{\sigma c} \tag{19}$$

where K_1, K_2, K_3, and K_4 are 3×3 symmetric positive definite matrices. The input vectors $\underline{v}_{\rho c}$ and $\underline{v}_{\sigma c}$ are the variables of commands. If $\underline{v}_{\rho c} = \underline{0}$ and $\underline{v}_{\sigma c} = \underline{0}$, we deal with the problem of regulation; otherwise, $\underline{\rho}_m$ and $\underline{\sigma}_m$ are the responses of a second-order system to the inputs $\underline{v}_{\rho c}$ and $\underline{v}_{\sigma c}$.

Defining the error variables $\underline{\varepsilon}_\rho = \underline{\rho} - \underline{\rho}_m$ and $\underline{\varepsilon}_\sigma = \underline{\sigma} - \underline{\sigma}_m$, between the spacecraft actual state and the evolution of Eq. (19), by using Eqs. (8), (12), (14), and (19), we obtain:

$$\begin{aligned} &\ddot{\underline{\varepsilon}}_\rho + K_1\dot{\underline{\varepsilon}}_\rho + K_2\underline{\varepsilon}_\rho = \frac{1}{m}{}^{L}R_S(\underline{\sigma})H_F\underline{u} - (\underline{v}_{\rho c} - \underline{v}_{\rho l});\\ &\ddot{\underline{\varepsilon}}_\sigma + K_3\dot{\underline{\varepsilon}}_\sigma + K_4\underline{\varepsilon}_\sigma = G(\underline{\sigma})H_M\underline{u} - (\underline{v}_{\sigma c} - \underline{v}_{\sigma l}) \end{aligned} \tag{20}$$

where $\underline{v}_{\rho l} = \underline{h}(\underline{\rho}, \dot{\underline{\rho}}) + K_1\dot{\underline{\rho}} + K_2\underline{\rho}$ and

$$\underline{v}_{\sigma l} = \underline{f}(\underline{\sigma}, \dot{\underline{\sigma}}, \underline{\omega}_L, \dot{\underline{\omega}}_L) + K_3\dot{\underline{\sigma}} + K_4\underline{\sigma}$$

We rearrange Eq. (20) by introducing the variables $\underline{e}_\rho = [\,\underline{\varepsilon}_\rho \quad \dot{\underline{\varepsilon}}_\rho\,]^T$, $\underline{e}_\sigma = [\,\underline{\varepsilon}_\sigma \quad \dot{\underline{\varepsilon}}_\sigma\,]^T$, and $\underline{e} = [\,\underline{e}_\rho \quad \underline{e}_\sigma\,]^T$:

$$\dot{\underline{e}} = A_m\underline{e} + B(\underline{\sigma})(H\underline{u} - \underline{w}) \tag{21}$$

with

$$A_m = \begin{bmatrix} A_{1m} & 0_{3\times3} \\ 0_{3\times3} & A_{2m} \end{bmatrix}; \quad A_{1m} = \begin{bmatrix} 0_{3\times3} & I_{3\times3} \\ -K_1 & -K_2 \end{bmatrix}; \quad A_{2m} = \begin{bmatrix} 0_{3\times3} & I_{3\times3} \\ -K_3 & -K_4 \end{bmatrix} \tag{22}$$

and

$$B(\underline{\sigma}) = \begin{bmatrix} 0_{3\times3} & 0_{3\times3} \\ \frac{1}{m}{}^{L}R_S(\underline{\sigma}) & 0_{3\times3} \\ 0_{3\times3} & 0_{3\times3} \\ 0_{3\times3} & G(\underline{\sigma}) \end{bmatrix}; \qquad \underline{w} = \begin{bmatrix} \underline{w}_F \\ \underline{w}_M \end{bmatrix} = \begin{bmatrix} m{}^{L}R_S(-\underline{\sigma})(\underline{v}_{\rho c} - \underline{v}_{\rho l}) \\ G^{-1}(\underline{\sigma})(\underline{v}_{\sigma c} - \underline{v}_{\sigma l}) \end{bmatrix} \tag{23}$$

Equation (21) is the reference model tracking error equation, where the matrices A_{1m} and A_{2m} and, therefore, A_m are Hurwitz [21]. It is noteworthy that, if $H\underline{u} = \underline{w}$ in Eq. (21), the system of Eq. (15) has the dynamics $\ddot{\underline{\rho}} + K_1\dot{\underline{\rho}} + K_2\underline{\rho} = \underline{v}_{\rho c}$ and $\ddot{\underline{\sigma}} + K_3\dot{\underline{\sigma}} + K_4\underline{\sigma} = \underline{v}_{\sigma c}$. In fact, in Eq. (21) the term $(H\underline{u} - \underline{w})$ forces the dynamics of the tracking error. If this term is zero, the tracking error goes exponentially to zero. The variables $\underline{w}_F$ and $\underline{w}_M$ can be seen as the ideal controls to yield the linear behavior of the system in Eq. (15).

B. Lyapunov Approach

To study the stability of Eq. (21) under the thrusters' actuation, we use the Lyapunov approach by selecting as a candidate function:

$$V(\underline{e}) = \underline{e}^T P\underline{e} \tag{24}$$

with $P = P^T > 0$. Differentiating Eq. (24) along the trajectories in Eq. (21), we find:

$$\tfrac{\mathrm{dV}}{\mathrm{dt}} = \underline{e}^T(A_m P + PA_m^T)\underline{e} + 2\underline{e}^T PB(\underline{\sigma})(H\underline{u} - \underline{w}) \tag{25}$$

For a specified symmetric positive definite matrix Q, the matrix P is found as the unique solution of the Lyapunov equation:

$$A_m P + PA_m^T = -Q \tag{26}$$

and Eq. (21) is asymptotically stable if $2\underline{e}^T PB(\underline{\sigma})(H\underline{u} - \underline{w}) \le 0$. In particular, in order to separate the position error contribution from the attitude error contribution, if we select:

$$Q = \begin{bmatrix} Q_1 & 0_{6\times6} \\ 0_{6\times6} & Q_2 \end{bmatrix} \tag{27}$$

with $Q_1 = Q_1^T > 0$ and $Q_2 = Q_2^T > 0$, Eq. (26) has the solution of the form [22]:

$$P = \begin{bmatrix} P_\rho & 0_{6\times6} \\ 0_{6\times6} & P_\sigma \end{bmatrix} \tag{28}$$

By partitioning the matrices P_ρ and P_σ as

$$P_\rho = \begin{bmatrix} P_{\rho1} & P_{\rho2} \\ P_{\rho2}^T & P_{\rho3} \end{bmatrix}; \qquad P_\sigma = \begin{bmatrix} P_{\sigma1} & P_{\sigma2} \\ P_{\sigma2}^T & P_{\sigma3} \end{bmatrix} \tag{29}$$

Equation (25) yields:

$$\tfrac{\mathrm{dV}}{\mathrm{dt}} = -\underline{e}_\rho^T Q_1\underline{e}_\rho - \underline{e}_\sigma^T Q_2\underline{e}_\sigma + 2\Delta \tag{30}$$

where

$$\begin{aligned} &\Delta = \Delta_\rho + \Delta_\sigma; \qquad \Delta_\rho = \underline{\gamma}_\rho^T(H_F\underline{u} - \underline{w}_F);\\ &\Delta_\sigma = \underline{\gamma}_\sigma^T(H_M\underline{u} - \underline{w}_M);\\ &\underline{\gamma}_\rho^T = (\underline{\varepsilon}_\rho^T P_{\rho2} + \dot{\underline{\varepsilon}}_\rho^T P_{\rho3})\tfrac{1}{m}{}^{L}R_S(\underline{\sigma}) = \tfrac{1}{m}\underline{e}_\rho^T K_\rho^{T}{}^{L}R_S(\underline{\sigma});\\ &\underline{\gamma}_\sigma^T = (\underline{\varepsilon}_\sigma^T P_{\sigma2} + \dot{\underline{\varepsilon}}_\sigma^T P_{\sigma3})G(\underline{\sigma}) = \underline{e}_\sigma^T K_\sigma^T G(\underline{\sigma}) \end{aligned} \tag{31}$$

with $K_\rho = [\,P_{\rho2} \quad P_{\rho3}\,]^T$ and $K_\sigma = [\,P_{\sigma2} \quad P_{\sigma3}\,]^T$. Equation (30) implies that the tracking error $\underline{e} \to \underline{0}$ if $\Delta \le 0$.

Table 1 Components of $\underline{\beta}_\rho$ and $\underline{\beta}_\sigma$

Thruster	1	2	3	4	5	6	7	8	9	10	11	12
$\underline{\beta}_\rho^T =$	$-\varphi_1$	φ_2	φ_3	$-\varphi_1$	$-\varphi_2$	$-\varphi_3$	φ_1	φ_2	$-\varphi_3$	φ_1	$-\varphi_2$	φ_3
$\underline{\beta}_\sigma^T =$	$-\pi_1$	π_5	$-\pi_6$	π_1	π_2	π_3	π_4	$-\pi_5$	$-\pi_3$	$-\pi_4$	$-\pi_2$	π_6

C. Selection of the Active Thrusters' Configuration

We seek to establish the asymptotic stability of the reference model tracking error equation (21) under a suitable selection of the thrusters to be activated. From Eq. (31), we rearrange the two relations using the vector of the active thrusters' configuration $\hat{\underline{u}}$:

$$\Delta_\rho = \underline{\beta}_\rho^T \hat{\underline{u}} - \delta_F; \qquad \Delta_\sigma = \underline{\beta}_\sigma^T \hat{\underline{u}} - \delta_M \tag{32}$$

with

$$\underline{\beta}_\rho^T = u_a \underline{\gamma}_\rho^T H_F; \qquad \underline{\beta}_\sigma^T = u_a \underline{\gamma}_\sigma^T H_M; \qquad \delta_F = \underline{\gamma}_\rho^T \underline{w}_F; \qquad \delta_M = \underline{\gamma}_\sigma^T \underline{w}_M \tag{33}$$

By using the first relation of Eqs. (31) and (32), we can therefore write:

$$\Delta = (\underline{\beta}_\rho^T \hat{\underline{u}} - \delta_F) + (\underline{\beta}_\sigma^T \hat{\underline{u}} - \delta_M) \tag{34}$$

To make Δ zero or negative, we have to find the suitable binary vector $\hat{\underline{u}}$. It is easy to see that, if $\delta_F + \delta_M \geq 0$, no thrusters must be activated (that is, $\hat{\underline{u}} = \underline{0}$), because the condition $\Delta \leq 0$ is automatically satisfied.

From Eqs. (17) and (18) of the submatrices H_F and H_M and Eq. (31), we find the vectors $\underline{\beta}_\rho$ and $\underline{\beta}_\sigma$ and write Table 1.

In the first row of Table 1, the identification number of the thruster is listed, and the functions φ_i and π_j are

$$\begin{bmatrix} \varphi_1 \\ \varphi_2 \\ \varphi_3 \end{bmatrix} = \begin{pmatrix} u_a & 0 & 0 \\ 0 & u_a & 0 \\ 0 & 0 & u_a \end{pmatrix} \begin{bmatrix} \gamma_{\rho 1} \\ \gamma_{\rho 2} \\ \gamma_{\rho 3} \end{bmatrix} \tag{35}$$

$$\begin{bmatrix} \pi_1 \\ \pi_2 \\ \pi_3 \\ \pi_4 \\ \pi_5 \\ \pi_6 \end{bmatrix} = \begin{pmatrix} 0 & -u_a d_z & u_a d_y \\ u_a d_z & 0 & -u_a d_x \\ -u_a d_y & u_a d_x & 0 \\ 0 & u_a d_z & u_a d_y \\ u_a d_z & 0 & u_a d_x \\ u_a d_y & u_a d_x & 0 \end{pmatrix} \begin{bmatrix} \gamma_{\sigma 1} \\ \gamma_{\sigma 2} \\ \gamma_{\sigma 3} \end{bmatrix} \tag{36}$$

Looking at Table 1, the vectors $\underline{\beta}_\rho$ and $\underline{\beta}_\sigma$ can be written as

$$\underline{\beta}_\rho = \underline{b}_\rho(\underline{\varphi}); \qquad \underline{\beta}_\sigma = \underline{b}_\sigma(\underline{\pi}) \tag{37}$$

where $\underline{\varphi}^T = [\varphi_1 \quad \varphi_2 \quad \varphi_3]$ and $\underline{\pi}^T = [\pi_1 \quad \pi_2 \quad \pi_3 \quad \pi_4 \quad \pi_5 \quad \pi_6]$, while $\underline{b}_\rho$ maps $\underline{\varphi}$ into $\underline{\beta}_\rho$, and $\underline{b}_\sigma$ maps $\underline{\pi}$ into $\underline{\beta}_\sigma$.

If $\delta_F + \delta_M < 0$, three cases are found to yield the suitable active thrusters' configuration $\hat{\underline{u}}$.

1. *Selection of the Active Thrusters' Configuration when $\delta_F < 0$ and $\delta_M \geq 0$*

We search a thrusters' configuration that makes $\Delta \leq 0$ and, because $\delta_M \geq 0$, that implies $\Delta_\sigma \leq 0$; the configuration does not have to introduce any control torque (that is, $\underline{\beta}_\sigma^T \hat{\underline{u}} = 0$). The thrusters to be selected belong to the configuration $\hat{\underline{u}}_F$, for which $\beta_{\rho k} < 0$ for $k = 1, 2, \ldots, 12$ and, due to property 1 (see Sec. II.B.4), it provides a control force only (see Table 1). We must demonstrate that the selected configuration $\hat{\underline{u}}_F$ yields $\Delta_\rho \leq 0$. Table 1 shows that a set of components $\underline{\beta}_\rho$ are always negative, because the functions φ_i are either positive or negative; if all these functions equal zero, then [from Eq. (35)], the term Δ_ρ vanishes. Note that, for each function φ_i, a couple of thrusters are concerned. Assuming we select all the thrusters for which $\beta_{\rho k} < 0$, then by using Eqs. (32) and (33), we obtain:

$$\begin{aligned} \Delta_\rho = {} & (-2|\varphi_1| - \gamma_{\rho 1} w_{F1}) + (-2|\varphi_2| - \gamma_{\rho 2} w_{F2}) \\ & + (-2|\varphi_3| - \gamma_{\rho 3} w_{F3}) \end{aligned} \tag{38}$$

The most negative values of δ_F are when $\gamma_{\rho i} w_{Fi} < 0$, for $i = 1, 2, 3$; therefore, from the relation of Eq. (35) we have:

$$\begin{aligned} \Delta_\rho \leq {} & |\gamma_{\rho 1}|(-2u_a + |w_{F1}|) + |\gamma_{\rho 2}|(-2u_a + |w_{F2}|) \\ & + |\gamma_{\rho 3}|(-2u_a + |w_{F3}|) \end{aligned} \tag{39}$$

Thus, a sufficient condition to have $\Delta \leq 0$ is

$$|w_{Fi}| \leq 2u_a \quad \text{for } i = 1, 2, 3 \tag{40}$$

2. *Selection of the Active Thrusters' Configuration when $\delta_F \geq 0$ and $\delta_M < 0$*

We search a thrusters' configuration that makes $\Delta \leq 0$ and, because $\delta_F \geq 0$, that implies $\Delta_\rho \leq 0$; the configuration does not have to introduce any control force (that is, $\underline{\beta}_\rho^T \hat{\underline{u}} = 0$). The thrusters to be selected belong to the configuration $\hat{\underline{u}}_M$, for which $\beta_{\sigma k} < 0$ for $k = 1, 2, \ldots, 12$ and, due to property 2 (see Sec. II.B.4), such configuration provides control torque only (see Table 1). As in the previous case, we must demonstrate that the configuration $\hat{\underline{u}}_M$ yields $\Delta_\sigma \leq 0$. Table 1 shows that a set of components $\underline{\beta}_\sigma$ are always negative because the functions π_i are either positive or negative. In addition, each of these functions is related to a couple of thrusters; if all these functions equal zero, then [from Eq. (36)], the term Δ_σ vanishes. Assuming we select all the thrusters for which $\beta_{\sigma k} < 0$, by using Eqs. (32) and (33), we have:

$$\Delta_\sigma = -\sum_{j=1}^{6} |\pi_j| - \sum_{i=1}^{3} \gamma_{\sigma i} w_{Mi} \tag{41}$$

The most negative values of δ_M are when $\gamma_{\sigma i} w_{Mi} < 0$ for $i = 1, 2, 3$; therefore,

$$\Delta_\sigma \leq -\sum_{j=1}^{6} |\pi_j| + \sum_{i=1}^{3} |\gamma_{\sigma i} w_{Mi}| \tag{42}$$

By using Eq. (36), we obtain the relation:

$$\begin{aligned} \Delta_\sigma \leq {} & |\gamma_{\sigma 1}| \cdot [-2u_a(d_z + d_y) + |w_{M1}|] + + |\gamma_{\sigma 2}| \\ & \cdot [-2u_a(d_z + d_x) + |w_{M2}|] + + |\gamma_{\sigma 3}| \cdot [-2u_a(d_y + d_x) + |w_{M3}|] \end{aligned} \tag{43}$$

Thus, a sufficient condition to have $\Delta \leq 0$ is

$$\begin{gathered} |w_{M1}| \leq 2u_a(d_z + d_y); \qquad |w_{M2}| \leq 2u_a(d_z + d_x); \\ |w_{M3}| \leq 2u_a(d_y + d_x) \end{gathered} \tag{44}$$

Table 2 Switching table for φ_1, π_1, and π_4

	$\pi_1 > 0$	$\pi_1 < 0$	$\pi_4 > 0$	$\pi_4 < 0$
$\varphi_1 > 0$	1	4	——	——
$\varphi_1 < 0$	——	——	10	7

Table 3 Switching table for φ_2, π_2, and π_5

	$\pi_2 > 0$	$\pi_2 < 0$	$\pi_5 > 0$	$\pi_5 < 0$
$\varphi_2 > 0$	11	5	——	——
$\varphi_2 < 0$	——	——	8	2

Table 4 Switching table for φ_3, π_3, and π_6

	$\pi_3 > 0$	$\pi_3 < 0$	$\pi_6 > 0$	$\pi_6 < 0$
$\varphi_3 > 0$	9	6	——	——
$\varphi_3 < 0$	——	——	3	12

3. Selection of the Active Thrusters' Configuration when $\delta_F < 0$ and $\delta_M < 0$

In this case, the activation rule needs to consider both vectors $\underline{\beta}_\rho$ and $\underline{\beta}_\sigma$. In fact, we search an active thrusters' configuration $\underline{\hat{u}}_T$ that provides control force and torque at the same time. The rule follows the same strategy of the above cases, because the aim is to select thrusters that provide negative weights in the sums:

$$\sum_{k=1}^{12} \beta_{\rho k} \hat{u}_{Tk}$$

and

$$\sum_{k=1}^{12} \beta_{\sigma k} \hat{u}_{Tk}$$

Assume that $\varphi_1 > 0$ (see Table 1); if $\pi_1 > 0$, then thruster 1 must be activated (that is, generating a force component along the opposite direction of the x axis, a negative torque component around the z axis, and a positive torque component around the y axis) (see Fig. 2). If $\pi_1 < 0$, then thruster 4 must be activated, thus leading to a similar discussion (as mentioned before) of opposite signs of the torque components. We can recursively repeat the same statements for all of the other combinations of the functions φ_i and π_j of Table 1, which are positive or negative according to the tracking error behavior. As a consequence, we can construct three switching tables (Tables 2–4). In these tables, the number k identifies that the kth thruster must be activated.

The switching tables show that the activation rule does not set on a couple of thrusters, as in the cases of Secs. III.C.1 and III.C.2, but one only. This implies that $\Delta \leq 0$ as a sufficient condition, if

$$|w_{Fi}| \leq u_a; \qquad i = 1, 2, 3 \tag{45}$$

and

$$\begin{gathered} |w_{M1}| \leq u_a(d_z + d_y); \qquad |w_{M2}| \leq u_a(d_z + d_x); \\ |w_{M3}| \leq u_a(d_y + d_x) \end{gathered} \tag{46}$$

D. Asymptotic Stability of the Tracking Error Dynamics

The analysis of the previous section provides the selection of the rules to activate the suitable thrusters. Moreover, we have found sufficient conditions for which the asymptotic stability of the tracking error dynamics are achieved. Notice that the sufficient conditions of Eqs. (45) and (46) dominate the sufficient conditions of Eqs. (40) and (44). As a result, if the inequalities of Eqs. (45) and (46) are satisfied, the active thrusters' configurations found in Sec. III.C guarantee that the tracking error $\underline{e} \to 0$. Actually, the tracking error cannot reach zero; however, it reaches a residual set around the equilibrium, which is the limit cycle in the case of a periodic orbit of convergence [23]. This is because the actuators are on–off devices and have a minimum in the duration of the pulse.

The conditions of the asymptotic stability to a residual set are the admissible range values that the ideal controls, w_{Fi} and w_{Mi}, must have. The ideal controls are not known a priori, because they are functions of the actual states $\underline{\rho}$ and $\underline{\sigma}$ of the system controlled by the thrusters' activations [Eq. (23)]. Anyhow, w_{Fi} and w_{Mi} can be predicted by computing them on the designed behaviors $\underline{\rho}_m$ and $\underline{\sigma}_m$. If they are not in the admissible ranges, it means that the thrusters in hand have a lower thrust than the necessary to track the desired behaviors of $\underline{\rho}_m$ and $\underline{\sigma}_m$. Therefore, we have to change the behaviors of $\underline{\rho}_m$ and $\underline{\sigma}_m$ [for instance, by reducing the values of the gain matrices in Eq. (19)] until the conditions of Eqs. (45) and (46) are verified. If the designed behaviors of $\underline{\rho}_m$ and $\underline{\sigma}_m$ are mandatory, it implies the need of thrusters with a higher thrust to be taken into account during the spacecraft design process. As the simulation will show, under the conditions of Eqs. (45) and (46) for $\underline{\rho}_m$ and $\underline{\sigma}_m$, and assuming that the initial conditions of the real dynamics [Eq. (15)] and those of the reference models [Eq. (19)] are the same, the controlled dynamics are not far from the behavior of the reference models. This is because the selected active thrusters' configuration makes the derivative of the Lyapunov function of Eq. (25) negative and, as a consequence, the tracking error $\underline{e}$ is kept within the region that includes the residual set of asymptotic stability around the equilibrium.

E. Algorithms to Minimize the Active Thrusters

This section deals with the problem of minimizing the number of the thrusters to be activated, aiming at the condition $\Delta \leq 0$. The algorithms assume that the inequalities of Eqs. (45) and (46) are met

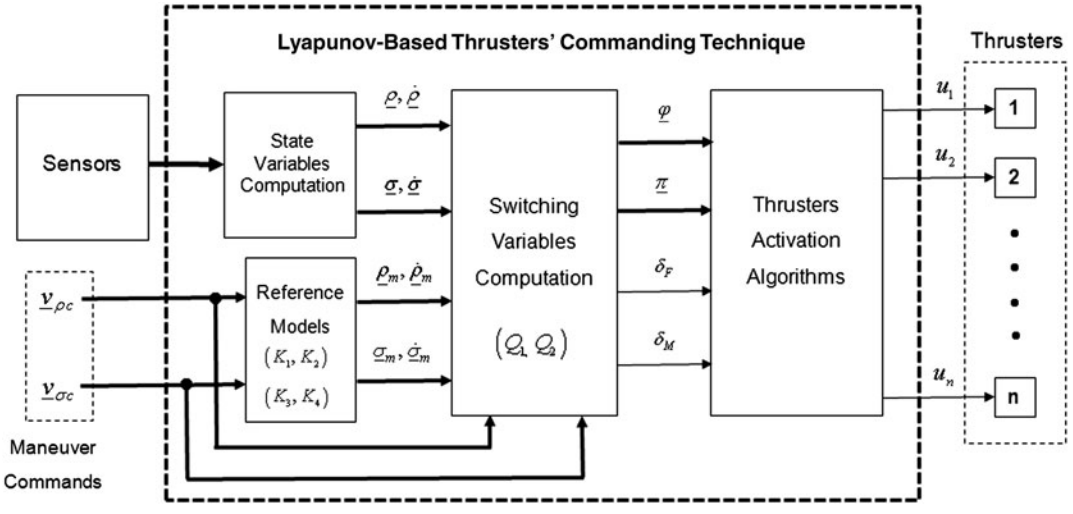

Fig. 4 Block diagram of the proposed control method.

Table 5 Spacecraft parameters

Mass	$m = 500$ kg
Size	$L_x = 1.5$ m; $L_y = 2$ m; $L_z = 2.5$ m
Moments of inertia	$J_x = 427$ kg · m^2; $J_y = 354$ kg · m^2; $J_z = 260.4$ kg · m^2
Thrusters' placement	$d_x = L_x/2$; $d_y = L_y/2$; $d_z = L_z/2$
Thrust	$u_a = 2$ N
Minimum pulse duration (valves mechanical limit)	50 ms

and use of the selection rules of Sec. III.C. Let $S(a)$ be the switching function:

$$S(a) = \begin{cases} 1 & a < 0 \\ 0 & a \geq 0 \end{cases} \tag{47}$$

If $\delta_F + \delta_M < 0$, we must consider three activation algorithms:

1) $\delta_F < 0$ and $\delta_M \geq 0$.

a) Initialize the vectors $\underline{\hat{\varphi}} = \underline{0}$ and $\underline{\tilde{\varphi}} = \underline{\varphi}$;

b) Let φ_i be the function of $\underline{\tilde{\varphi}}$ that has the maximum absolute value; then we set $\hat{\varphi}_i = \varphi_i$ and $\tilde{\varphi}_i = 0$.

c) Compute $\underline{\hat{\beta}}_\rho = \underline{b}_\rho(\underline{\hat{\varphi}})$.

d) Compute $\hat{u} = [\, S(\hat{\beta}_{\rho 1}) \quad S(\hat{\beta}_{\rho 2}) \quad \cdots \quad S(\hat{\beta}_{\rho k}) \quad \cdots \quad S(\hat{\beta}_{\rho 12})]^T$.

e) If $\Delta = (\underline{\beta}_\rho^T \underline{\hat{u}} - \delta_F - \delta_M) \leq 0$ then stop, else go to b.

2) $\delta_F \geq 0$ and $\delta_M < 0$.

a) Initialize the vectors $\underline{\hat{\pi}} = \underline{0}$ and $\underline{\tilde{\pi}} = \underline{\pi}$.

b) Let π_j be the function of $\underline{\tilde{\pi}}$ that has the maximum absolute value; then we set $\hat{\pi}_j = \pi_j$ and $\tilde{\pi}_j = 0$.

c) Compute $\underline{\hat{\beta}}_\sigma = \underline{b}_\sigma(\underline{\hat{\pi}})$.

d) Compute $\hat{u} = [\, S(\hat{\beta}_{\sigma 1}) \quad S(\hat{\beta}_{\sigma 2}) \quad \cdots \quad S(\hat{\beta}_{\sigma k}) \quad \cdots \quad S(\hat{\beta}_{\sigma 12})]^T$.

e) If $\Delta = (\underline{\beta}_\sigma^T \underline{\hat{u}} - \delta_F - \delta_M) \leq 0$ then stop, else go to b.

3) $\delta_F < 0$ and $\delta_M < 0$.

a) Initialize the vectors $\underline{\hat{\beta}} = \underline{0}$ and $\underline{\tilde{\beta}} = \underline{0}$.

b) Find the matching components in the vectors $\underline{\beta}_\rho$ and $\underline{\beta}_\sigma$, for which $\beta_{\rho k} < 0$ and $\beta_{\sigma k} < 0$, and compute $\tilde{\beta}_k = \beta_{\rho k} + \beta_{\sigma k}$.

c) Let h be the position of the most negative value of $\underline{\tilde{\beta}}$; then we set $\hat{\beta}_h = \tilde{\beta}_h$ and $\tilde{\beta}_h = 0$.

d) Compute $\hat{u} = [\, S(\hat{\beta}_1) \quad S(\hat{\beta}_2) \quad \cdots \quad S(\hat{\beta}_k) \quad \cdots \quad S(\hat{\beta}_{12})]^T$.

e) If $\Delta = (\underline{\beta}^T \underline{\hat{u}} - \delta_F - \delta_M) \leq 0$, then stop; else go to c.

The maximum number of iterations is three for algorithm 1 and six for 2 and 3. The time of thrusting is the time in which the sign of $\delta_F + \delta_M$ is negative, while the signs of δ_F and δ_M switch among the thrusters' activation algorithms 1, 2, and 3.

F. Control Law Design

The suitable configuration $\underline{\hat{u}}$ is found under the constraints of Eqs. (45) and (46). The design of the control law has to take into account these constraints to yield, as a sufficient condition, a stable tracking control. From Eq. (23), it is recognizable that the expressions of the variables $\underline{w}_F$ and $\underline{w}_M$ are the linearizing control functions of the translational dynamics [Eq. (11)] and the rotational dynamics [Eq. (7)]. In fact, in Eq. (12), if ${}^S\underline{F}_c = \underline{w}_F$ (and recalling that ${}^L\underline{F}_c = {}^L R_S(\underline{\sigma})\, {}^S\underline{F}_c$), then the translational dynamics become

$$\ddot{\underline{\rho}} + K_1 \dot{\underline{\rho}} + K_2 \underline{\rho} = \underline{v}_{\rho c} \tag{48}$$

and, in Eq. (8) if ${}^S\underline{M}_c = \underline{w}_M$, then the rotational dynamics become

$$\ddot{\underline{\sigma}} + K_3 \dot{\underline{\sigma}} + K_4 \underline{\sigma} = \underline{v}_{\sigma c} \tag{49}$$

In point of fact, the linearizing controls $\underline{w}_F$ and $\underline{w}_M$ are not applied to the system and they are only used in the expressions of δ_F and δ_M [see Eq. (33)].

In the case of regulation, the input variables are $\underline{v}_{\rho c} = \underline{0}$ and $\underline{v}_{\sigma c} = \underline{0}$. If a desired trajectory maneuver $\underline{\rho}_d(t)$ is required [from Eq. (19)], we can use the variable $\underline{v}_{\rho c}$ with the law:

$$\underline{v}_{\rho c} = \ddot{\underline{\rho}}_d + K_1 \dot{\underline{\rho}}_d + K_2 \underline{\rho}_d \tag{50}$$

Similarly, if an attitude maneuver $\underline{\sigma}_d(t)$ is planned, we can use the variable $\underline{v}_{\sigma c}$ with the law:

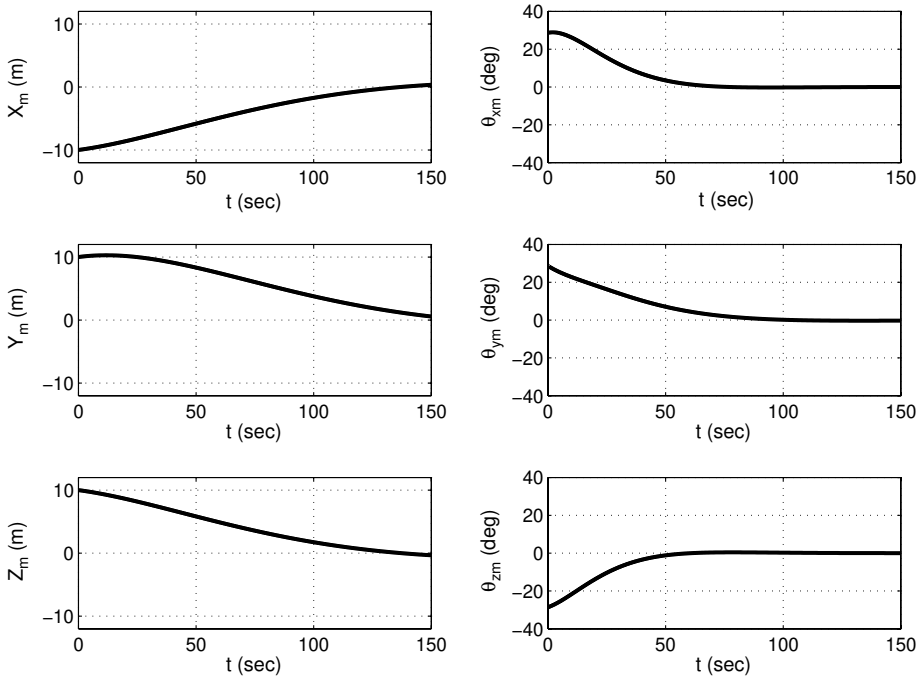

Fig. 5 Reference model behavior for the spacecraft center of mass and spacecraft attitude.

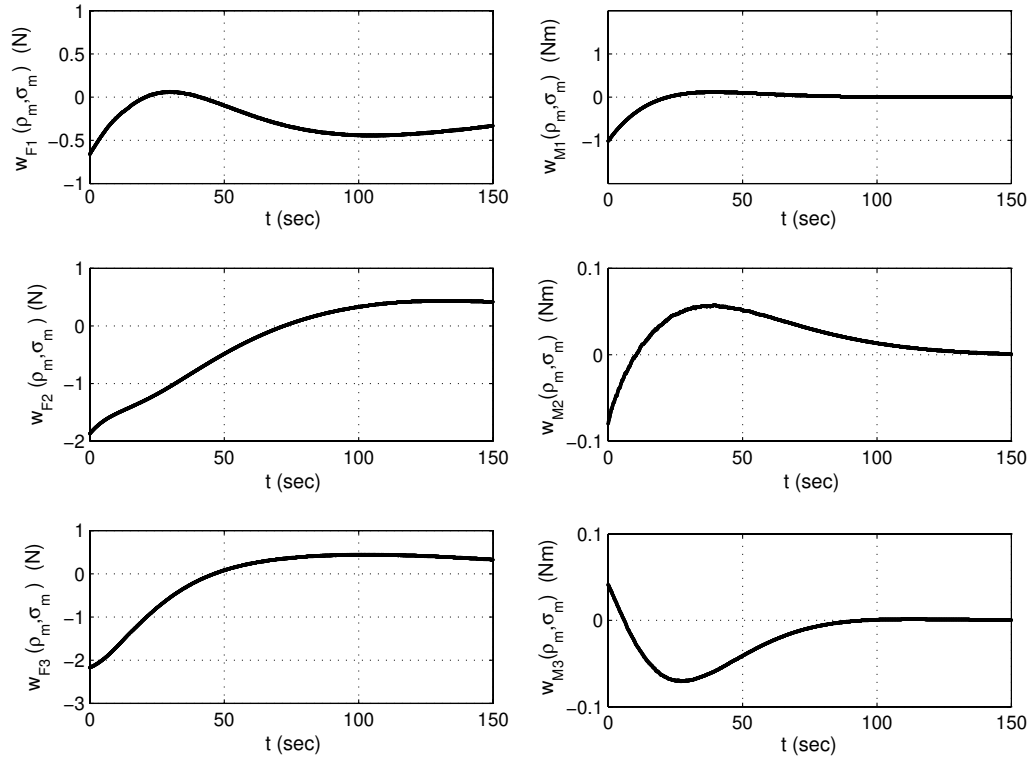

Fig. 6 Functions $\underline{w}_F$ and $\underline{w}_M$ vs time for the reference model.

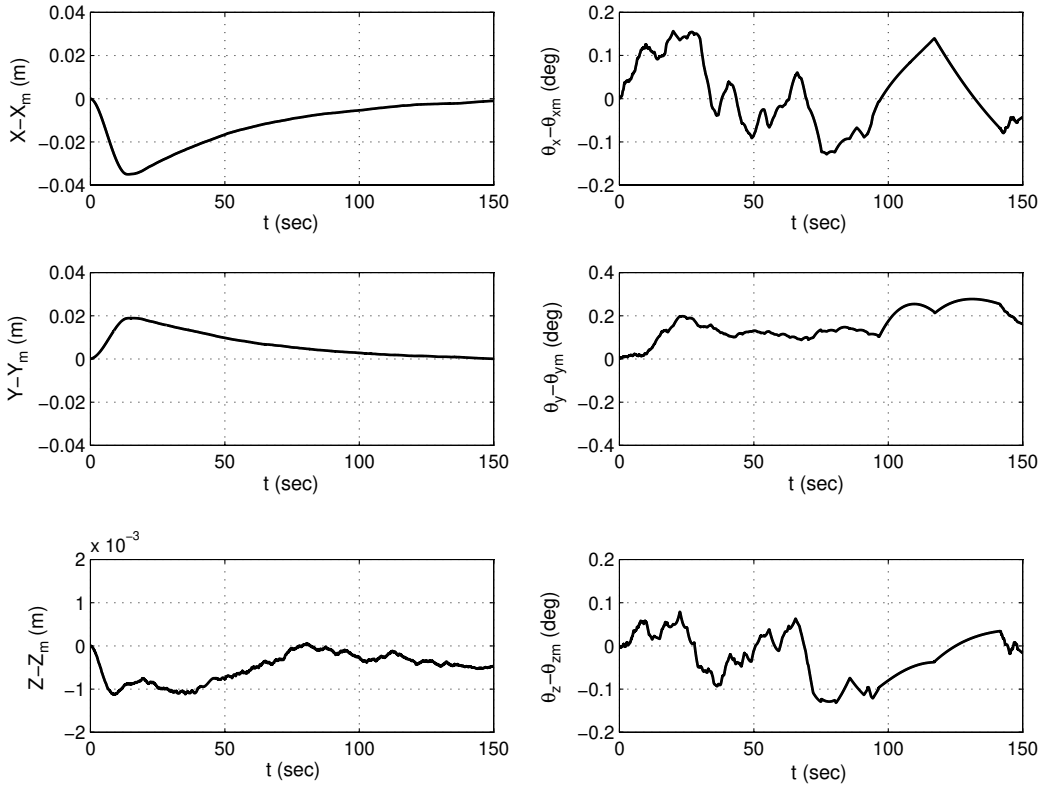

Fig. 7 Numerical simulation result: spacecraft center of mass position and attitude tracking errors.

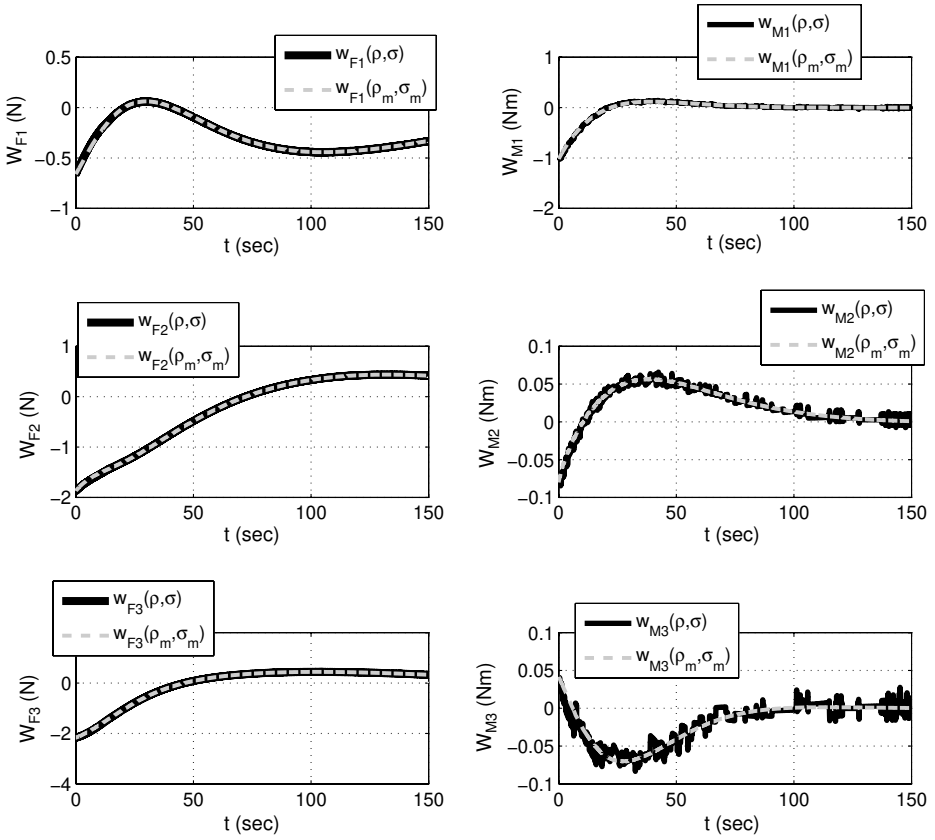

Fig. 8 Numerical simulation result: functions $\underline{w}_F$ and $\underline{w}_M$ comparisons vs time.

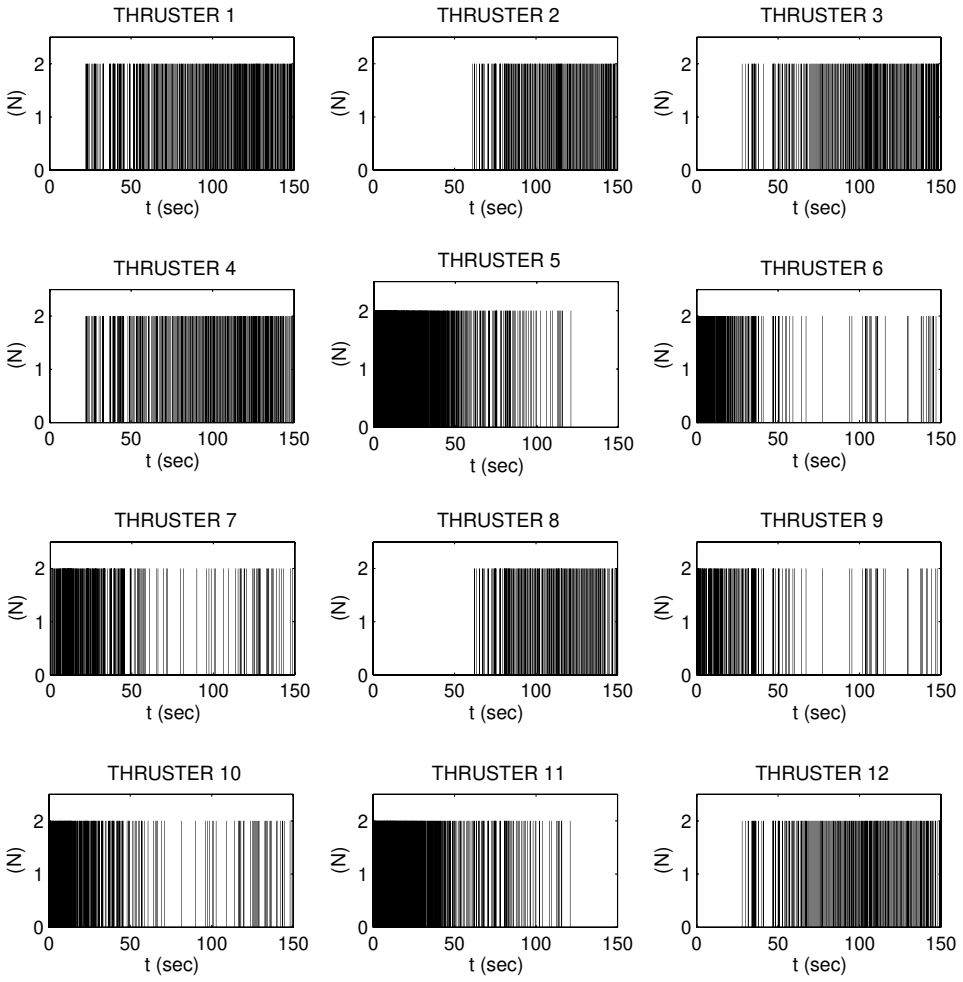

Fig. 9 Numerical simulation result: thrusters' commands history.

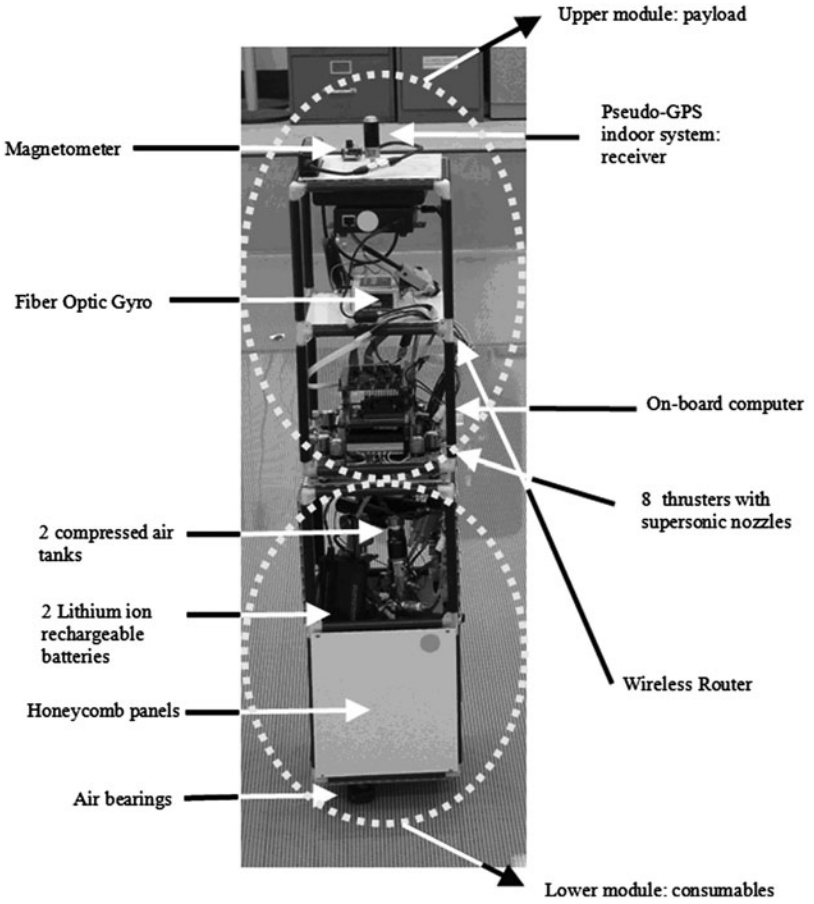

Fig. 10 Spacecraft simulator at the Spacecraft Robotics Laboratory, Naval Postgraduate School.

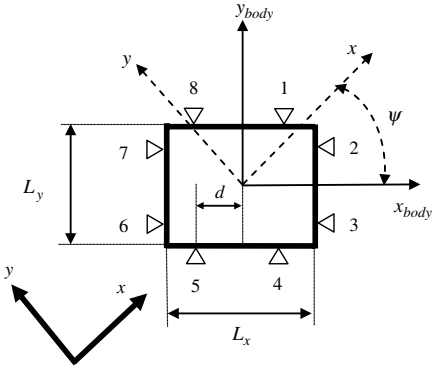

Fig. 11 Spacecraft simulator representative sketch.

$$\underline{v}_{\sigma c} = \ddot{\underline{\sigma}}_d + K_3\dot{\underline{\sigma}}_d + K_4\underline{\sigma}_d \tag{51}$$

The command strategy devised in Sec. III.C ensures, for the position and attitude variables of the space vehicle, that $\underline{\rho} \to \underline{\rho}_m$ while $\underline{\rho}_m \to \underline{\rho}_d$ and $\underline{\sigma} \to \underline{\sigma}_m$ while $\underline{\sigma}_m \to \underline{\sigma}_d$.

A block diagram of the proposed control method is reported in Fig. 4.

The advantages of using the proposed method with respect to the classical control approach are as follows:

1) The required behavior of on–off controlled rototranslational dynamics can be designed by choosing suitable linear dynamics.

2) The computational complexity in searching the thrusters' configuration is reduced with respect to the solving simplex problem (see Sec. II.C). This last point can be clarified by exploring the algorithms devised for solving the minimization problem formulated in Sec. II.C, which uses iterative sequences of matrix operations [24].

IV. Simulation Results: Proximity Operation of a Spacecraft

In this section, we apply the proposed model reference method to the problem of the proximity navigation of a spacecraft. The objective of the spacecraft is to zero out its position and velocity, as well as its attitude and angular rates, with respect to the LVLH reference frame that is attached to the orbiting point on a circular orbit with the semimajor axis of 9800 km.

A. Reference Model and Control Design

The spacecraft parameters are summarized in Table 5, where (from Fig. 2) L_x, L_y, and L_z are the size of the vehicle along the body reference axes.

The model reference dynamics equations (19) have the matrices:

$$K_1 = 2.4 \cdot 10^{-2} \cdot I_{3\times3}; \qquad K_2 = 3.6 \cdot 10^{-3} \cdot I_{3\times3};$$
$$K_3 = \mathrm{diag}\{\,0.1 \quad 0.06 \quad 0.096\,\}; \tag{52}$$
$$K_4 = 10^{-3}\mathrm{diag}\{\,3.7 \quad 1.3 \quad 3.7\,\}$$

Table 6 Spacecraft simulator parameters

Mass	$m = 10.5$ kg
Size	$L_x = 19$ cm; $L_y = 19$ cm
Moment of inertia	$J_z = 0.032$ kg · m^2
Thrusters' placement	$d = 5$ cm
Thrust	$u_a = 0.159$ N
Minimum pulse duration (valves mechanical limit)	50 ms

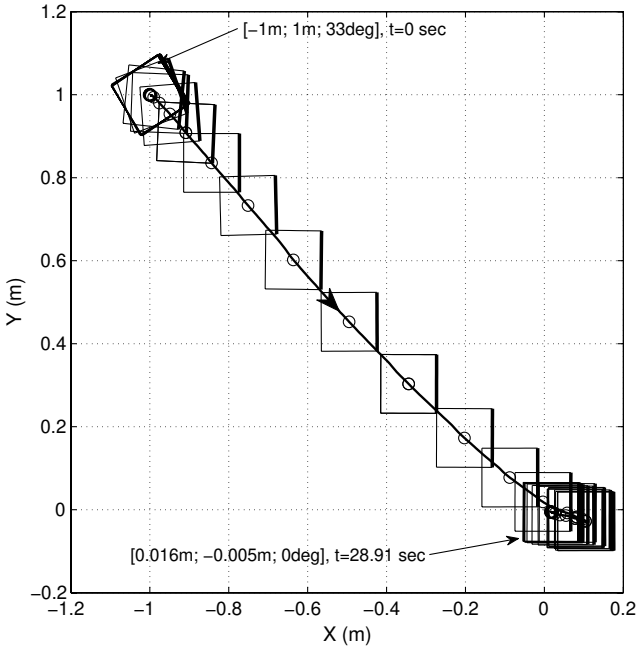

Fig. 12 Experimental result: bird's eye view for experiment 1: regulation. The bold side of the square is used to visualize the heading of the spacecraft simulator.

The designed behavior of the reference dynamics are plotted in Fig. 5, where θ_x, θ_y, and θ_z are the 1-2-3 Euler angles that represent the attitude of the SRF with respect to the LVLH frame. The reference trajectories and maneuvers are obtained as the integration of Eq. (19), with $\underline{v}_{\rho c} = \underline{0}$ and $\underline{v}_{\sigma c} = \underline{0}$ starting from the initial conditions: $x_m = -10$ m, $y_m = 10$ m, $z_m = 10$ m; velocities $\dot{x}_m = 0.05$ m/s, $\dot{y}_m = 0.05$ m/s, and $\dot{z}_m = -0.05$ m/s; Euler angles $\theta_{xm} = 30$ deg, $\theta_{ym} = 30$ deg, and $\theta_{zm} = -30$; and angular velocities $\omega_{xm} = 6$ deg/s, $\omega_{ym} = -6$ deg/s, and $\omega_{zm} = 6$ deg/s.

As explained in Sec. III.C, the inequalities of Eqs. (45) and (46) need to be verified; in this case, by using the values of Table 1, we have:

$$|w_{Fi}| \leq 2 \text{ N}; \qquad i = 1, 2, 3 \tag{53}$$

$$|w_{M1}| \leq 4.5 \text{ Nm}; \qquad |w_{M2}| \leq 4 \text{ Nm}; \qquad |w_{M3}| \leq 3.5 \text{ Nm} \tag{54}$$

The functions $\underline{w}_F$ and $\underline{w}_M$ are computed on $\underline{\rho}_m$, and $\underline{\sigma}_m$ and the behaviors are shown in Fig. 6.

It can be easily seen that these functions are in the ranges defined by Eqs. (53) and (54); therefore, the Lyapunov-based thruster selection strategy ensures the stability condition of the tracking error.

B. Simulation Results

Simulations are conducted by choosing the matrices in Eq. (27):

$$Q_1 = 5 \cdot 10^4 \cdot I_{3\times 3}; \qquad Q_2 = 5 \cdot 10^5 \cdot I_{3\times 3} \tag{55}$$

Figure 7 shows the position errors and the attitude errors. As discussed in Sec. III.C, the initial conditions of the reference models in Eq. (19) have been taken as the initial conditions of the real dynamics in Eq. (15); which is the reason for the initial errors' value of zero.

As Fig. 7 shows, the errors' values are kept small and, as a result, the spacecraft tracks the reference models. The tracking errors reach a residual set about zero because of the nonlinear nature of the problem related to the on–off actuators.

Figure 8 depicts the behavior of the components of $\underline{w}_F$ and $\underline{w}_M$ as functions of $\underline{\rho}_m$, $\underline{\sigma}_m$, and $\underline{\rho}$, $\underline{\sigma}$. The comparisons show that the difference among the values is small, which implies (as pointed our previously) that the designed control can be tested on the reference models' behavior to verify the inequalities (45) and (46).

Figure 9 shows the history of the thrusters' activation; the computed total impulse for the maneuver is 313 Ns.

V. Planar Case: Laboratory Experiments with a Floating Spacecraft Simulator

The experimental tests included in this paper have been conducted by using one of the floating spacecraft simulators (see Fig. 10) at the flat floor test bed of the Naval Postgraduate School. This three-degree-of-freedom simulator has size of $0.19 \times 0.19 \times 0.81$ m and a mass of 10.5 kg. It has a magnetometer, a gyroscope, and a pseudoglobal positioning system as sensors, and it has on–off cold-gas thrusters as actuators ([14,25–27]).

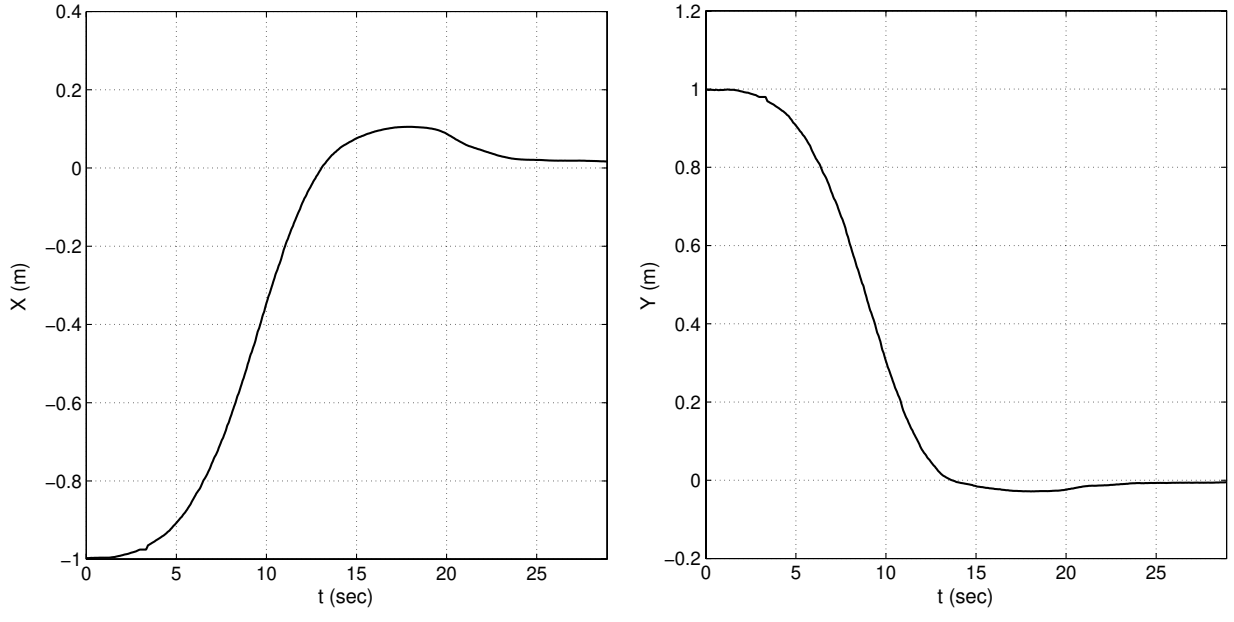

Fig. 13 Experimental result: x and y coordinates vs time for experiment 1, regulation.

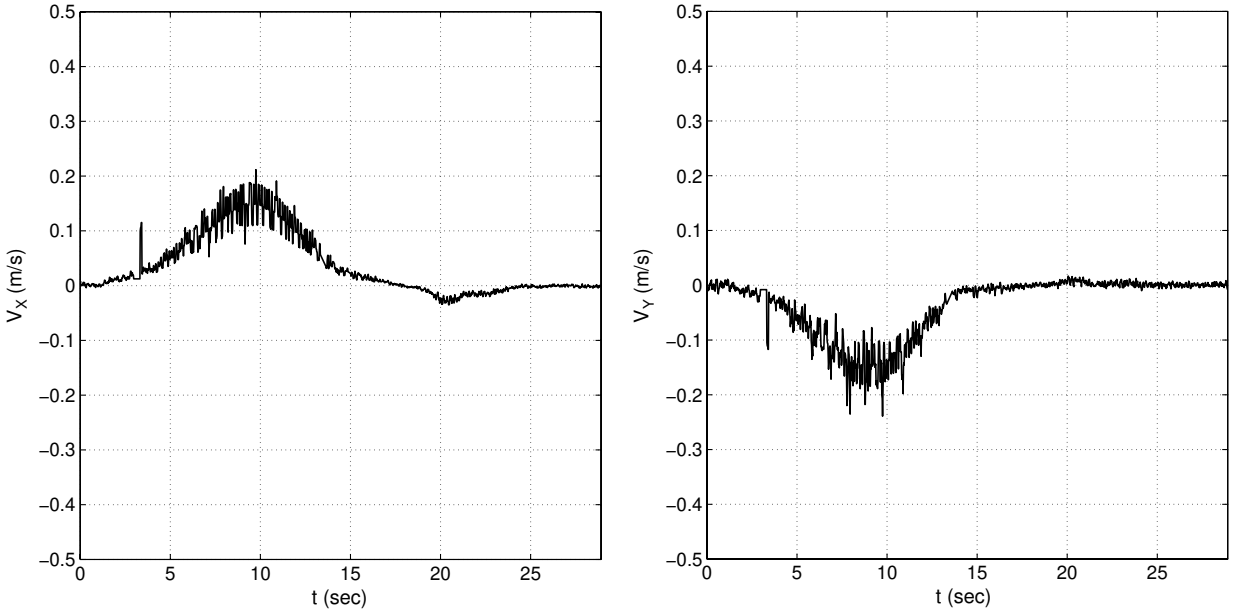

Fig. 14 Experimental result: V_x and V_y vs time for experiment 1, regulation.

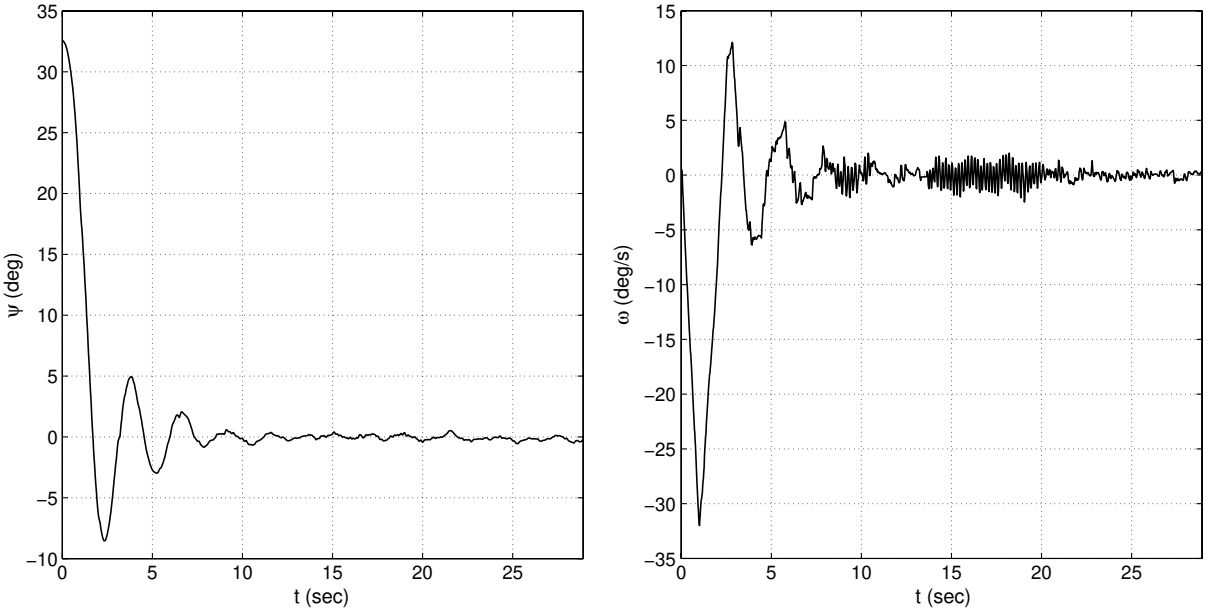

Fig. 15 Experimental result: ψ and ω vs time for experiment 1, regulation.

A. Spacecraft Simulator Model

The spacecraft simulator model is sketched in Fig. 11.

In Fig. 11, the frame (x, y) is the inertial reference frame, the frame $(x_{\text{body}}, y_{\text{body}})$ is the body reference frame, while ψ is the orientation angle of the spacecraft with respect to the local reference; the thrusters are numbered from 1 through 8 and are placed around the platform at a distance of d from the center of mass. The robot simulates in three-degree-of-freedom the rototranslational dynamics of a space vehicle and the main parameters are shown in Table 6.

From Eqs. (17) and (18), the submatrices of the thrust distribution matrix H have the structure:

$$H_F = \begin{bmatrix} 0 & -1 & -1 & 0 & 0 & 1 & 1 & 0 \\ -1 & 0 & 0 & 1 & 1 & 0 & 0 & -1 \end{bmatrix} \tag{56}$$

$$H_M = [-d \quad d \quad -d \quad d \quad -d \quad d \quad -d \quad d] \tag{57}$$

Let $\underline{\xi} = [x \quad y \quad \psi]^T$ be the vector of the generalized displacements, the rototranslational dynamics are

$$\ddot{\underline{\xi}} = \begin{pmatrix} \frac{1}{m}{}^I R_B(\psi) & 0_{2\times 1} \\ 0_{1\times 2} & \frac{1}{J_z} \end{pmatrix} H \underline{u} \tag{58}$$

where ${}^I R_B(\psi)$ is the rotation matrix from the local reference frame to the body reference frame and $\underline{u}$ is the vector defined in Eq. (13).

The β vectors of Table 1, used by the Lyapunov-based thruster selection strategy, become

$$\underline{\beta}_\rho^T = [-\varphi_2 \quad -\varphi_1 \quad -\varphi_1 \quad \varphi_2 \quad \varphi_2 \quad \varphi_1 \quad \varphi_1 \quad -\varphi_2] \tag{59}$$

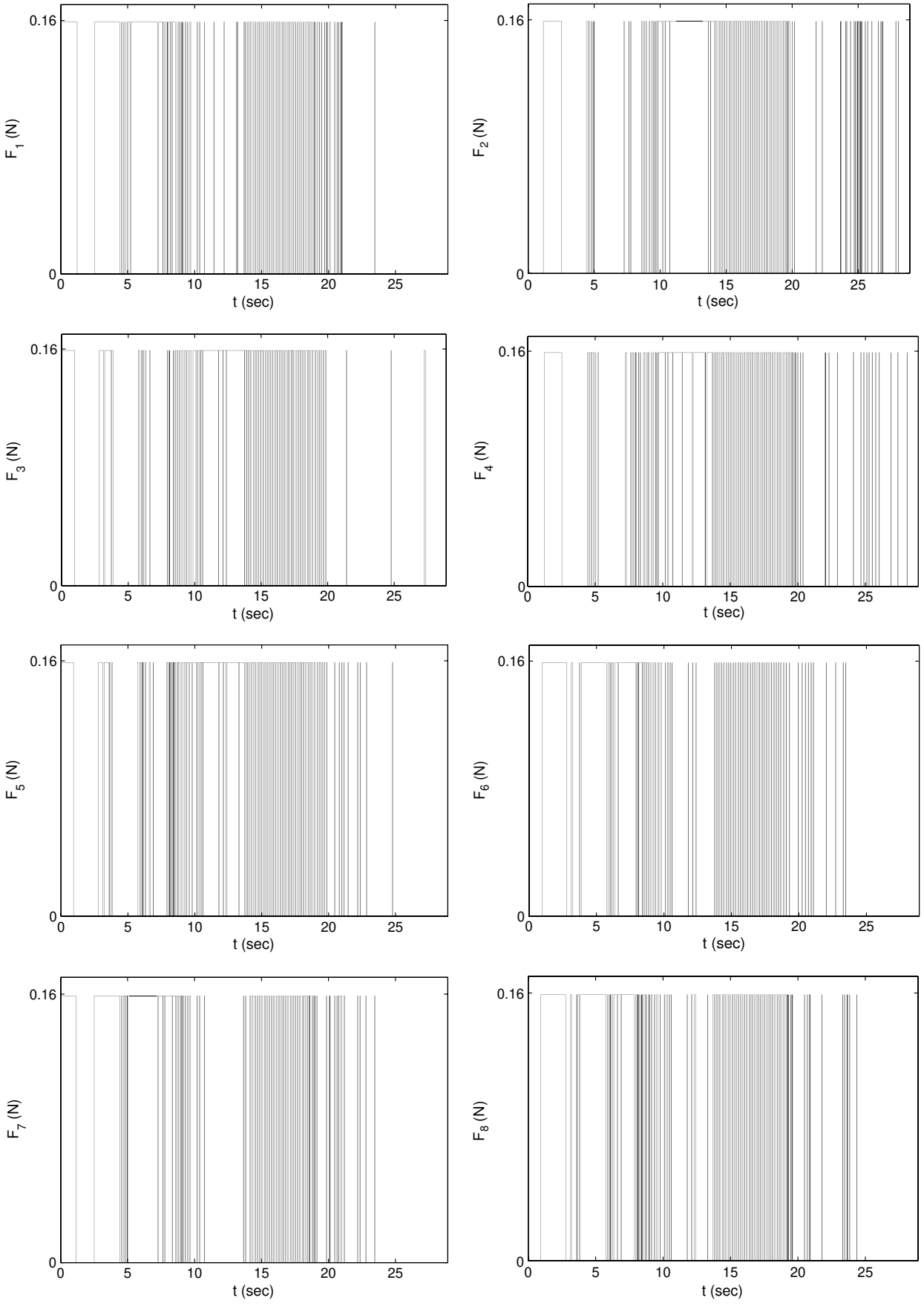

Fig. 16 Experimental result: thrusters' commands history for experiment 1, regulation.

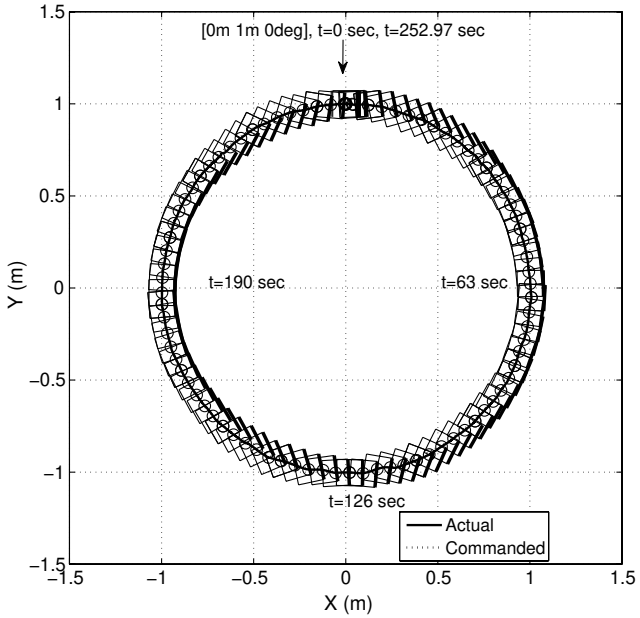

Fig. 17 Experimental result: bird's eye view for experiment 2, trajectory tracking. The bold side of the square is used to visualize the heading of the spacecraft simulator.

$$\underline{\beta}_{\sigma}^{T} = [-\pi \quad \pi \quad -\pi \quad \pi \quad -\pi \quad \pi \quad -\pi \quad \pi] \tag{60}$$

where

$$\underline{\varphi} = \begin{bmatrix} \varphi_1 \\ \varphi_2 \end{bmatrix} = \begin{pmatrix} u_a & 0 \\ 0 & u_a \end{pmatrix} \begin{bmatrix} \gamma_{\rho 1} \\ \gamma_{\rho 2} \end{bmatrix} = u_a \underline{\gamma}_{\rho} \tag{61}$$

$$\pi = d u_a \gamma_{\psi} \tag{62}$$

in which $\underline{\gamma}_{\rho}$ has the same meaning of Eq. (31), while γ_{ψ} is the variable related to the tracking error of the attitude represented by the angle ψ, instead of the MRPs in Eq. (31).

B. Control Design

The control design is based on the imposing of the reference trajectory $\underline{\rho}_m$ and maneuver ψ_m as solutions of the equations:

$$\ddot{\underline{\rho}}_m + K_1 \dot{\underline{\rho}}_m + K_2 \underline{\rho}_m = \underline{v}_{\rho c}; \qquad \ddot{\psi}_m + K_3 \dot{\psi}_m + K_4 \psi_m = v_{\psi c} \tag{63}$$

where $\underline{\rho} = [x \quad y]^T$, and on the selection of the matrices of the Lyapunov equation Eq. (26).

For the floating platform the following control matrices have been set to

$$K_1 = 10.6 \cdot I_{2\times 2}; \qquad K_2 = 35.13 \cdot I_{2\times 2}; \qquad K_3 = 0.24; \qquad K_4 = 0.5 \tag{64}$$

and

$$Q_1 = \mathrm{diag}\{1 \quad 1 \quad 10 \quad 10\}; \qquad Q_2 = 10 \cdot I_{2\times 2} \tag{65}$$

C. Experimental Results

This section reports the results of two experimental tests performed by implementing the proposed approach. The first test is a regulation maneuver, that is, $\underline{v}_{\rho c} = 0$ and $v_{\psi c} = 0$, which is run in order to show the stability of the control approach. The spacecraft simulator starts maneuvering at nonzero initial conditions in position and attitude. It is left free to maneuver in order to reach the null state vector.

The second experiment is a trajectory tracking test, performed in order to show the control logic stability with respect to a time-varying commanded state vector.

1. Experiment 1: Regulation

The robot starts maneuvering from the initial state vector,

$$[x_0 \quad y_0 \quad \psi \quad \dot{x}_0 \quad \dot{y}_0 \quad \omega] = [-1\ \mathrm{m} \quad 1\ \mathrm{m} \quad 33\ \mathrm{deg} \quad 0\ \mathrm{m/s} \quad 0\ \mathrm{m/s} \quad 0\ \mathrm{deg/s}]$$

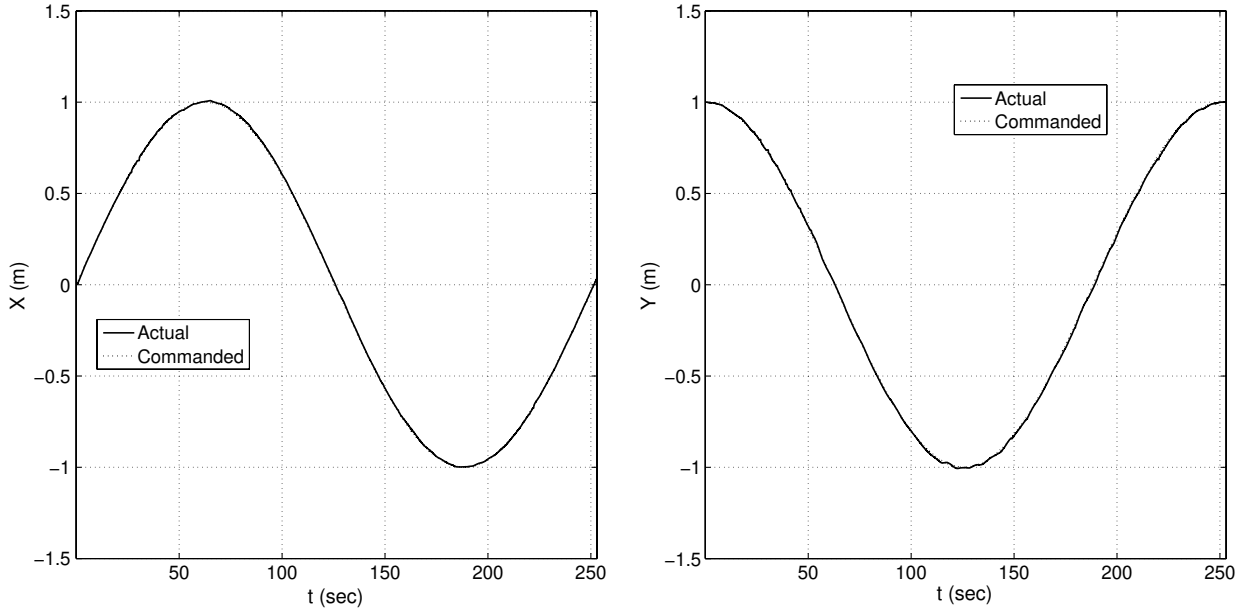

Fig. 18 Experimental result: *x* and *y* coordinates vs time for experiment 2, trajectory tracking.

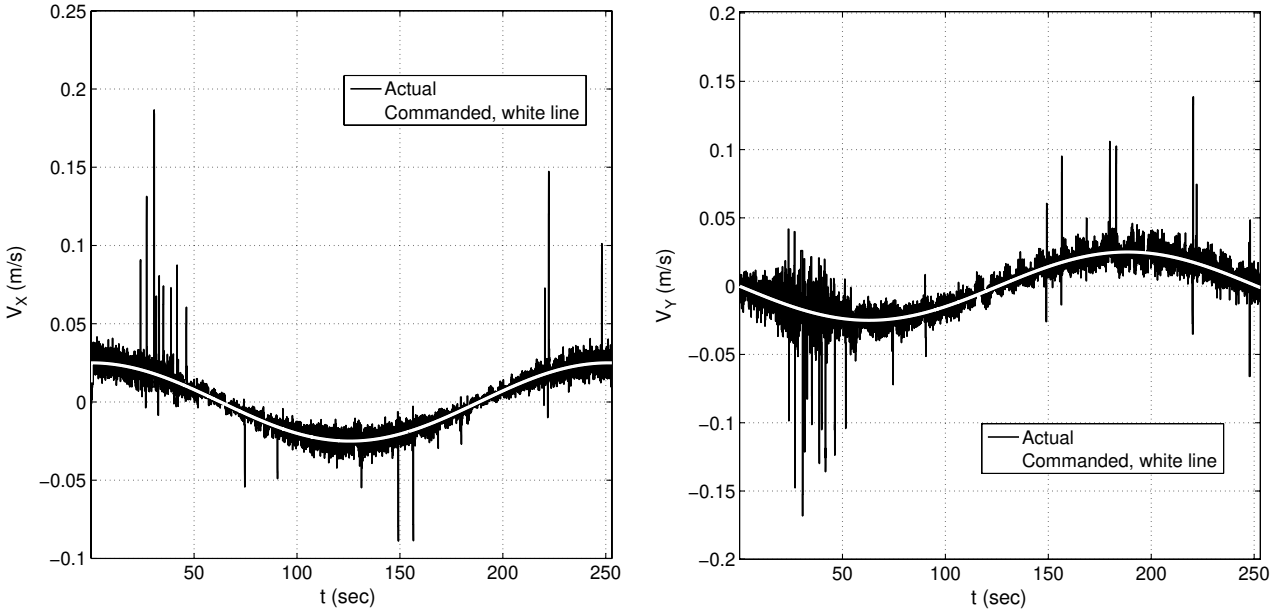

Fig. 19 Experimental result: V_x and V_y vs time for experiment 2, trajectory tracking.

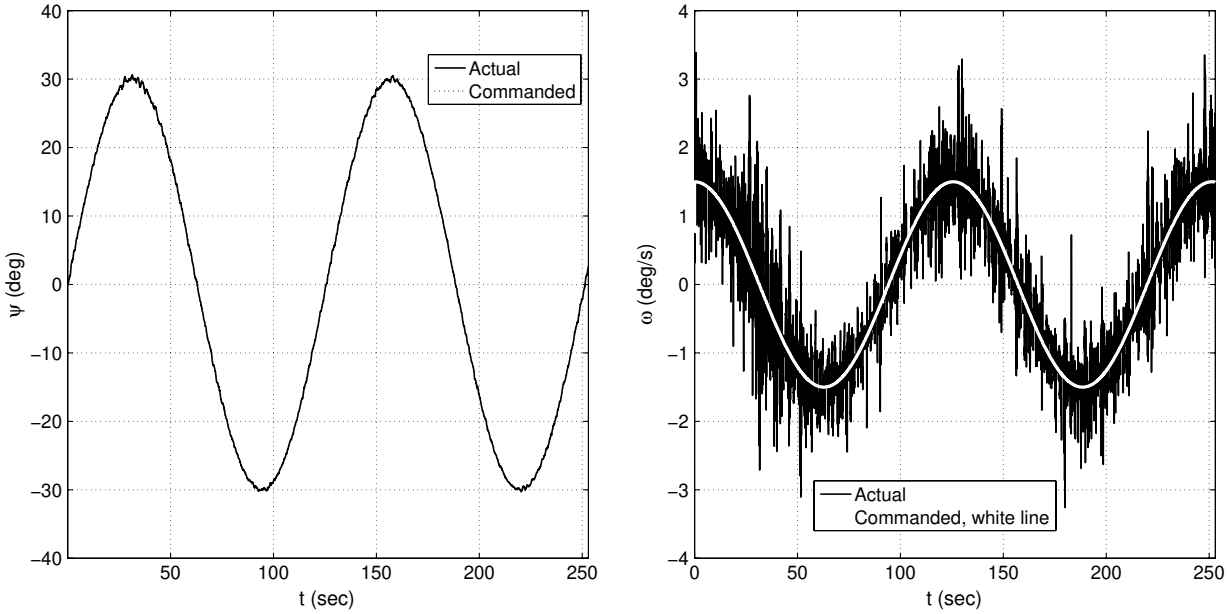

Fig. 20 Experimental result: ψ and ω vs time for experiment 2, trajectory tracking.

Table 7 Results of experiment 2

Total impulse	9.23 Ns
Mean of the tracking error in x	0.0025 m
Standard deviation in tracking error in x	0.0043 m
Mean of the tracking error in y	−0.0044 m
Standard deviation in tracking error in y	0.0155 m
Mean of the tracking error in V_x	0.0001 m/s
Standard deviation in tracking error in V_x	0.0075 m/s
Mean of the tracking error in V_y	0.0046 m/s
Standard deviation in tracking error in V_y	0.2139 m/s
Mean of the tracking error in ψ	0.0107 deg
Standard deviation in tracking error in ψ	0.2152 deg
Mean of the tracking error in ω	−0.0008 deg/s
Standard deviation in tracking error in ω	0.4160 deg/s

and it is intended to drive its state variables to zero. A video of the experimental run is available online.* The required impulse is 6.27 Ns and the required time is approximately 29 s. Figure 12 shows a bird's eye view of the regulation experiment with time tags at the start and end points. The bold side of the square is used to visualize the heading of the spacecraft simulator. The portions of the trajectories with sparse snapshots represent faster motion of the simulator on the flat floor (see also the video*). Figures 13 and 14 depict the behavior of the position and velocity components, while Fig. 15 shows the heading (angle about the vertical axis) and angular velocity. The simulator's motion closely follows the desired behavior of the linear reference model, with a minimal overshooting, as presented in Figs. 13 and 15.

The on–off sequences of the thrusters for the regulation experiments are reported in Fig. 16. The most of the on–off thrusting is concentrated at the beginning and at the end of the trajectory, while

*Data available online at http://vimeo.com/6599932 [retrieved 30 March 2010].

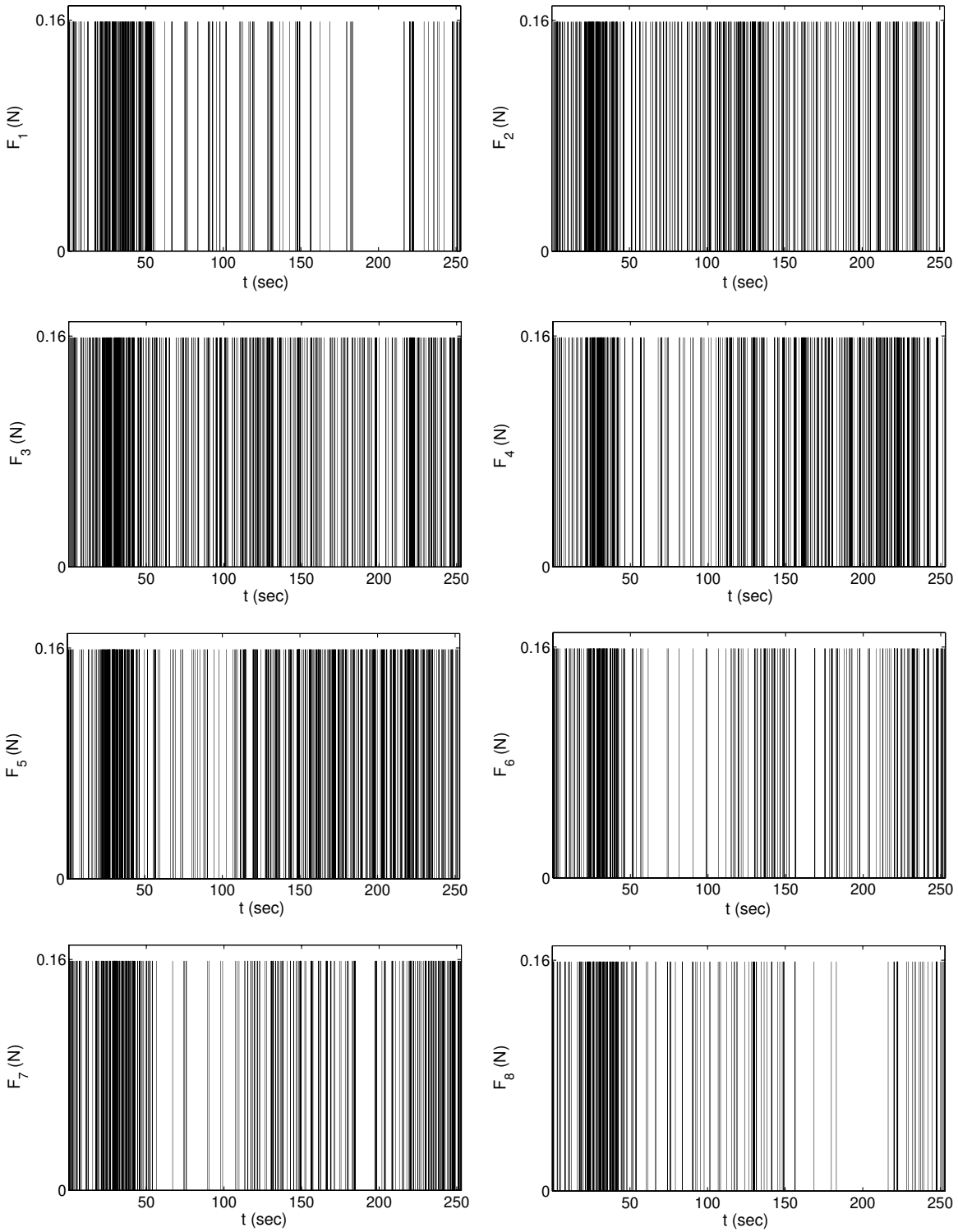

Fig. 21 Experimental result: thrusters' commands history for experiment 2, trajectory tracking.

the middle portion is characterized by longer intervals with the thrusters either on or off.

2. Experiment 2: Trajectory Tracking

The robot starts maneuvering from the initial state vector,

$$[x_0 \quad y_0 \quad \psi \quad \dot{x}_0 \quad \dot{y}_0 \quad \omega] = [0\ \text{m} \quad 1\ \text{m} \quad 0\ \text{deg} \quad 0\ \text{m/s} \quad 0\ \text{m/s} \quad 0\ \text{deg/s}]$$

and it is intended to track a 1 m radius circular trajectory at constant speed, while changing its attitude between 30 and −30 deg following a sine wave command. The commanded trajectory's frequency is $\varpi_\rho = 0.025$ rad/s, the angle's command frequency is $\varpi_\psi = 0.05$ rad/s. In this case, the command variable $\underline{v}_{\rho c}$ has the expressions of Eq. (50) with $\underline{\rho}_d^T = [\cos(\varpi_\rho t) \quad \sin(\varpi_\rho t)]$, while the command variable $v_{\psi c}$ has the expression of Eq. (51) with $\sigma_d = 0.5233\cos(\varpi_\psi t)$. This means that the circle is intended to be run in approximately 250 s while the angle's oscillation between 30 and −30 deg occurs twice within the same time frame. A video of the experimental run is available online.[†]

[†]Data available at http://vimeo.com/6600180 [retrieved 30 March 2010].

Figure 17 shows the bird's eye view of the experiment, the bold line is again employed to help visualizing the simulator's heading throughout the maneuver. Figure 18 shows the planar coordinates evolution in time, compared with the commanded signals. Figure 19 is dedicated to the comparison between commanded and actual planar velocities. Figure 20 is finally depicting the commanded heading and heading rate versus the experimental ones. In all the comparison plots a high tracking accuracy is achieved. Figure 21 collects the on–off history for the eight onboard thrusters.

Table 7 collects the main parameters related to the accuracy of the trajectory tracking and the total impulse for the maneuver.

In Figs. 14, 15, 19, and 20, a noisier behavior of the simulator's planar velocities and angular rate can be noticed, compared with the smooth behavior of the position and heading variables. This characteristic has to be ascribed to the navigation algorithms, whose behavior and tuning is beyond the scopes of this work. Nevertheless, the current navigation system allows for very satisfactory model tracking using the proposed control strategy.

VI. Conclusions

The Lyapunov-based thrusters' selection and commanding technique, presented in this paper, provides a method to control the rototranslational dynamics of a space vehicle with only on–off actuators by the tracking of linear reference models. The control design involves the choice of matrix coefficients of the linear reference models. The devised thruster selection strategy reduces the complexity of the classical approach because it replaces the thruster mapping and the PWF. The proposed strategy selects, at each time step, the thrusters to be fired, by checking the signs of functions of the tracking error. A minimum number of actuators is used.

The analysis yields the sufficient conditions for the asymptotic stability of the dynamics of the tracking error, which have to be imposed at each time step.

The paper establishes the stability of the method and presents numerical results for the six- degree-of-freedom case as well as experimental results by using three-degree-of-freedom floating spacecraft simulators.

Acknowledgment

This research was performed while R. Bevilacqua was holding a National Research Council Research Associateship Award at the Spacecraft Robotics Laboratory of the Naval Postgraduate School.

References

[1] Jackson, M., and Gonzales, R., "Orion Orbit Reaction Control Assessment," AIAA Guidance, Navigation and Control Conference and Exhibit, AIAA Paper 2007-6684, 2007.

[2] Izzo, D., and Pettazzi, L., "Autonomous and Distributed Motion Planning for Satellite Swarm," *Journal of Guidance, Control, and Dynamics*, Vol. 30, No. 2, March–April 2007, pp. 449–459. doi:10.2514/1.22736

[3] Subbarao, K., and Weish, S., "Nonlinear Control of Motion Synchronization for Satellite Proximity Operations," *Journal of Guidance, Control, and Dynamics*, Vol. 31, No. 5, Sept.–Oct. 2008, pp. 1284–1294. doi:10.2514/1.34248

[4] Luo, Y. Z., Tang, G. J., and Lei, Y. J., "Optimal Multi-Objective Linearized Impulsive Rendezvous," *Journal of Guidance, Control, and Dynamics*, Vol. 30, No. 2, March–April 2007, pp. 383–389. doi:10.2514/1.21433

[5] Swartwout, M., Scarritt S., and Neubauer, J., "Potential Function Controllers for Proximity Navigation of Underactuated Spacecraft," *Proceedings of the 30th Annual AAS Rocky Mountain Guidance and Control Conference*, American Astronautical Society Paper 07-043, Feb. 2007, pp. 267–286.

[6] Badawy, A., and McInnes, C. R., "On-Orbit Assembly Using Superquadric Potential Field," *Journal of Guidance, Control, and Dynamics*, Vol. 31, No. 1, Jan.–Feb. 2008, pp. 30–43. doi:10.2514/1.28865

[7] Dantzig, G. B., *Linear Programming and Extension*, Princeton Univ. Press, Princeton, NJ, 1998, pp. 94–146.

[8] Sidi, M. J., *Spacecraft Dynamics and Control: A Practical Engineering Approach*, Cambridge Univ. Press, Cambridge, England, U.K., 1997, pp. 265–289.

[9] Tohru Ieko, Yoshimasa Ochi, and Kimio Kanai, "New Design Method for Pulse-Width Modulation Control Systems via Digital Redesign," *Journal of Guidance, Control, and Dynamics*, Vol. 22, No. 1, 1999, pp. 123–128. doi:10.2514/2.4358

[10] Bernelli-Zazzera, F., Mantegazza, P., and Nurzia, V., "Multi-Pulse-Width Modulated Control of Linear Systems," *Journal of Guidance, Control, and Dynamics*, Vol. 21, No. 1, 1998, pp. 64–70. doi:10.2514/2.4198

[11] Robinet, R. D.,Parker, G. G., Schaub, H., and Junkins, J. L., "Lyapunov Optimal Saturated Control for Nonlinear Systems," *Journal of Guidance, Control, and Dynamics*, Vol. 20, No. 6, Nov.–Dec. 1997, pp. 1083–1088. doi:10.2514/2.4189

[12] Akella, M. R., Junkins, J. L., and Robinett, R. D., "Structured Model Reference Adaptive Control with Actuator Saturation Limit," AIAA/AAS Astrodynamics Specialist Conference and Exhibit, AIAA Paper 98-4472, Aug. 1998.

[13] Schaub, H., Akella, M. R., and Junkins, J. L., "Adaptive Control of Nonlinear Attitude Motions Realizing Linear Closed-loop Dynamics," *Proceedings of the American Control Conference*, 1999, pp. 1563–1567.

[14] Bevilacqua, R., Hall, J., Horning, J., Romano, M., "Ad-Hoc Wireless Networking and Shared Computation Based upon Linux for Autonomous Multi-Robot Systems," *Journal of Aerospace Computing, Information, and Communication*, Vol. 6, No. 5, May 2009, pp. 328–353. doi:10.2514/1.40734

[15] Shuster, M. D., "A Survey of Attitude Representations," *Journal of the Astronautical Sciences*, Vol. 41, No. 4, Oct.–Dec. 1993, pp. 439–517.

[16] Schaub, H., and Junkins, J. L., *Analytical Mechanics of Space Systems*, AIAA Educational Series, AIAA, Reston, VA, 2003, pp. 593–604.

[17] Melton, R. G., "Time-Explicit Representation of Relative Motion Between Elliptical Orbits," *Journal of Guidance, Control, and Dynamics*, Vol. 23, No. 4, 2000, pp. 604–610. doi:10.2514/2.4605

[18] Clohessy, W. H., and Wiltshire, R. S., "Terminal Guidance System for Satellite Rendezvous," *Journal of Aerospace Sciences*, Vol. 27, No. 9, Sept. 1960, pp. 653–658.

[19] Garus, J., "Optimal Allocation in the Propulsion System of an Underwater Vehicle," *International Journal of Applied Mathematics and Computer Sciences*, Vol. 14, No. 4, 2004, pp. 461–467.

[20] Yang, T., "Optimal Thrusters Selection with Robust Estimation for Formation Flying Applications," M.S. Thesis, Aeronautics and Astronautics, Massachusetts Inst. of Technology, Cambridge, MA, 2003.

[21] Khalil, H. K., *Nonlinear Systems*, 3rd ed., Prentice–Hall, Upper Saddle River, NJ, 2002, pp. 135–137.

[22] Gantmacher, F. R., *Matrix Theory*, Vol. 1, American Mathematical Society, Providence, RI, 2000, pp. 215–220.

[23] Bryson, A. E., Jr., *Control of Spacecraft and Aircraft*, Princeton Univ. Press, Princeton, N. J., 1994, pp. 28–36.

[24] Morgan, S. S., "A Comparison of Simplex Method Algorithms," M.S. Thesis, Univ. of Florida, Gainesville, FL, 1997.

[25] Hall, J. H., and Romano, M., "Robotic Testbed for the Experimentation of Guidance and Control of Spacecraft During Proximity Maneuvers," *Mechatronic Systems*, In-Tech, Vienna, Austria, 2009.

[26] Lugini, C., and Romano, M., "A Ballistic-Pendulum Test Stand to Characterize Small Cold-Gas Thruster Nozzles," *Acta Astronautica*, Vol. 64, Nos. 5–6, March-April 2009, pp. 615–625. doi:10.1016/j.actaastro.2008.11.001

[27] Romano, M., Friedman, D. A., and Shay, T. J., "Laboratory Experimentation of Autonomous Spacecraft Approach and Docking to a Collaborative Target," *Journal of Spacecraft and Rockets*, Vol. 44, No. 1, Jan.–Feb. 2007, pp. 164–173. doi:10.2514/1.22092